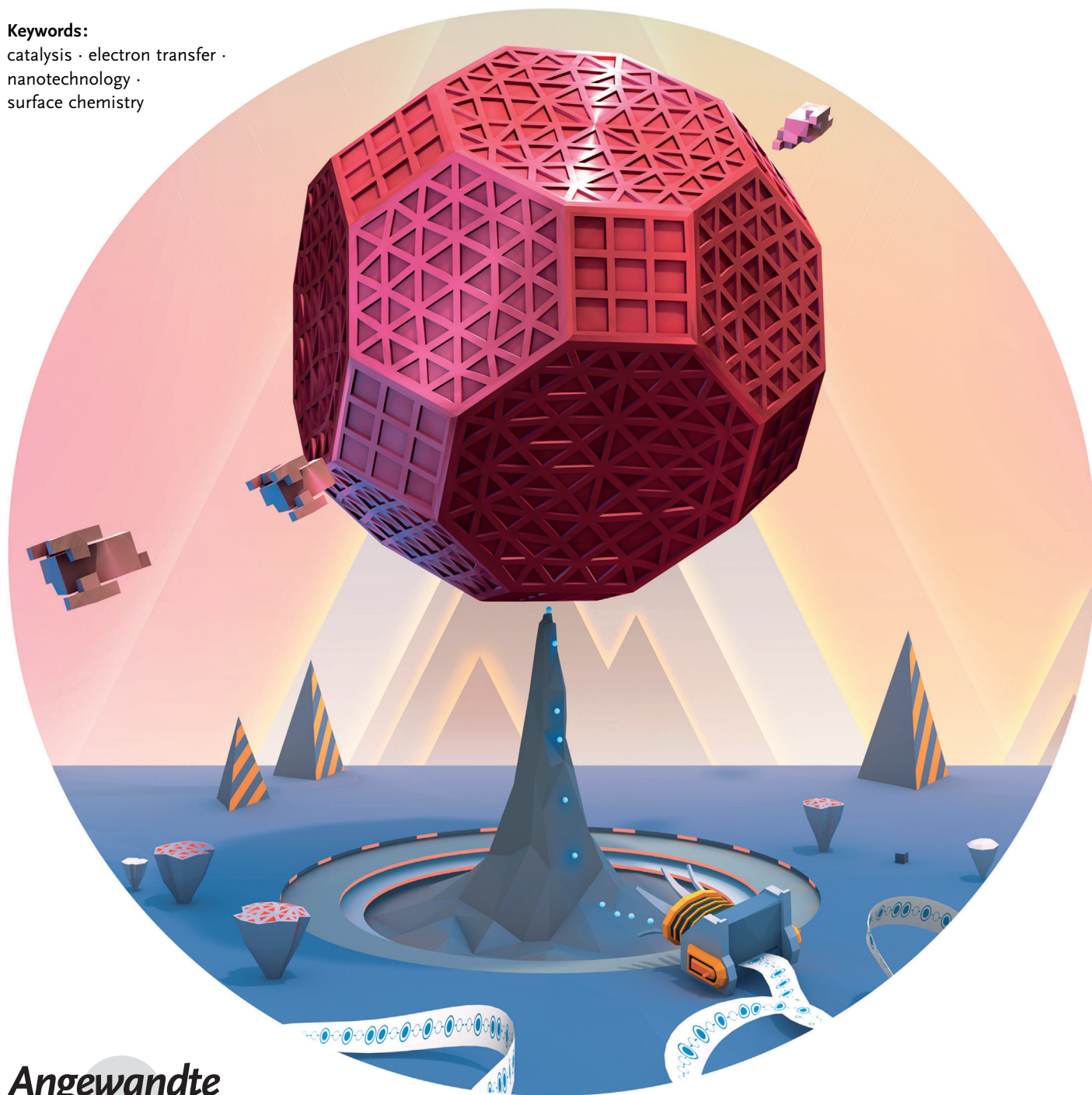


# Electrochemistry of Nanoparticles

*Steven E. F. Kleijn, Stanley C. S. Lai, Marc T. M. Koper,\* and Patrick R. Unwin\**

**Keywords:**

catalysis · electron transfer ·  
nanotechnology ·  
surface chemistry



**M**etal nanoparticles (NPs) find widespread application as a result of their unique physical and chemical properties. NPs have generated considerable interest in catalysis and electrocatalysis, where they provide a high surface area to mass ratio and can be tailored to promote particular reaction pathways. The activity of NPs can be analyzed especially well using electrochemistry, which probes interfacial chemistry directly. In this Review, we discuss key issues related to the electrochemistry of NPs. We highlight model studies that demonstrate exceptional control over the NP shape and size, or mass-transport conditions, which can provide key insights into the behavior of ensembles of NPs. Particular focus is on the challenge of ultimately measuring reactions at individual NPs, and relating the response to their structure, which is leading to imaginative experiments that have an impact on electrochemistry in general as well as broader surface and colloid science.

## 1. Introduction

Metal nanoparticles (NPs) have received a great deal of attention because of their fascinating physical and chemical properties, which can differ significantly from those of the bulk material. Interesting aspects of NPs include size- and shape-dependent interatomic bond distances,<sup>[1,2]</sup> melting points,<sup>[1,3]</sup> chemical reactivity,<sup>[4–6]</sup> and optical and electronic properties.<sup>[1,7,8]</sup> Furthermore, the small size of NPs has allowed nanoscale electrochemical processes to be probed, such as electric double layer effects on interfacial electron-transfer reactions.<sup>[9–12]</sup> NPs find many technical applications, such as in catalysis,<sup>[5,13,14]</sup> sensors,<sup>[15–17]</sup> and spectroscopy (such as surface-enhanced Raman spectroscopy),<sup>[17–19]</sup> as optical filters,<sup>[20]</sup> and in biomedical applications.<sup>[21–23]</sup>

Depending on the application in question, NPs are selected to achieve a particular function, from properties that emerge from both the constituent materials of the NP and its size. Significant research effort has thus aimed for a definitive understanding of the effect of shape and size on NP properties. In this context, electrochemical techniques are especially interesting, particularly when electrochemical characteristics can be related directly to other properties of the NPs. The challenge of ultimately measuring the electrochemical behavior of individual NPs is leading to imaginative experiments that have an impact on electrochemistry in general, as well as broader surface and colloid science, as we highlight in this Review.

One of the largest applications of NPs is in electrocatalysis, the field of catalysis concerned with reactions that involve charge transfer at the interface between a solid catalyst and an electrolyte.<sup>[13]</sup> This area is key to the development of fuel cells and batteries, electrolyzers, and electro-synthetic methods, as well as electrochemical sensing systems. The commercial viability of such devices requires the optimization of catalyst materials, not only to promote efficient use, but also to enhance selectivity towards a particular pathway.

## From the Contents

<b>1. Introduction</b>	3559
<b>2. Preparation and Characterization of Nanoparticulate Electrocatalysts</b>	3562
<b>3. Model Approaches to Real Catalysts</b>	3567
<b>4. Electrochemistry at Preferentially Shaped Nanoparticles</b>	3570
<b>5. Measurements of Individual Metal Nanoparticles</b>	3572
<b>6. Conclusions and Outlook</b>	3579

The reduction of particle size to decrease catalyst cost and improve usage does not necessarily lead to an optimal catalytic performance, as catalytic activity does not always scale linearly with the NP surface area. Ultrasmall NPs may become non-metal-like<sup>[24]</sup> and be more prone to poisoning,<sup>[25]</sup> and reaction pathways may depend strongly on the NP size.<sup>[26]</sup> Model (single-crystal) experiments<sup>[5,27]</sup> and computational studies<sup>[28]</sup> have shown that the interaction energies between reactant molecules and metal surface atoms depend strongly on the local arrangement of the metal atoms at the surface.

Moreover, the mass-transport rates of reactants, products, and intermediates depend significantly on the NP size and coverage on an electrode support. This makes the investigation of NP electrochemistry and electrocatalysis nontrivial, and, without proper controls, may lead to ambiguities when comparing data from different types of experiments (Section 3).

In fuel-cell applications, metal NP catalysts are supported on conductive carbon substrates and employed in membrane-electrode assemblies (MEAs; Figure 1 a). These real catalysts have been studied in model environments to evaluate their performance as a function of composition (Figure 1 b).<sup>[29]</sup> However, fuel-cell assemblies are complicated systems that suffer from, for example, fuel crossover across the membrane,

[\*] S. E. F. Kleijn, Prof. Dr. M. T. M. Koper  
Leiden Institute of Chemistry, Leiden University  
PO Box 9502, 2300 RA, Leiden (The Netherlands)  
E-mail: m.koper@chem.leidenuniv.nl  
Dr. S. C. S. Lai, Prof. Dr. P. R. Unwin  
Department of Chemistry, University of Warwick  
Gibbet Hill Road, Coventry CV4 7AL (UK)  
E-mail: p.r.unwin@warwick.ac.uk  
Dr. S. C. S. Lai  
Current address: MESA + Institute for Nanotechnology, University of Twente, PO Box 217, 7500 AE, Enschede (The Netherlands)

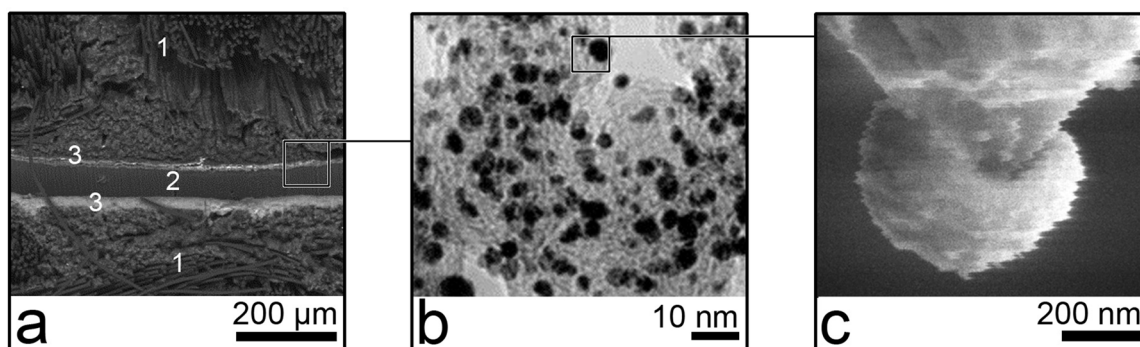


**Figure 1.** Different measurements on electrocatalysts: a) cross-section of a complete membrane-electrode assembly of a real catalyst in an application environment.<sup>[36]</sup> Gas-diffusion layers of a fibrous carbon cloth (1) sandwich a membrane (2) that has both anode and cathode catalyst layers (3) deposited on its sides (shown in light gray; 2004, Elsevier). b) A commercial Pt on C catalyst as used in studies of model environments (2005, Elsevier).<sup>[37]</sup> c) An individual, model Pt NP in a model environment (2003, American Chemical Society).<sup>[38]</sup>

non-electrochemical contributions to the cell-voltage, and an unknown and variable catalyst utilization factor.<sup>[30]</sup> Since these measurements leave the performance of individual NPs poorly understood, they are often complemented with studies on model catalysts. Model catalysts have tended to consist either of well-defined macroscopic metal electrodes or well-characterized dispersions of metal NPs on catalytically inert electrodes.

There are several recent developments that have allowed the focus of research to shift towards the study of individual NPs (Figure 1 c). We highlight how activity measurements on single NPs may ultimately provide the missing link between macroscopic electrodes and NP assemblies.

The use of NPs or nanoscale electrodes (NSEs) in electrochemistry has been the subject of various recent reviews, with a focus on electroanalysis,<sup>[15]</sup> NSEs and nanopores,<sup>[31–33]</sup> or NP synthesis.<sup>[34,35]</sup>

In this Review, we focus primarily on electrocatalysis at the level of individual NPs, assessing recently developed methods, including: advances in NP synthesis that allow the rational design of shape-controlled (faceted) NPs; novel electrochemical scanning probe methods that allow the study of single NPs; and recent developments in the detection of single NPs. To put these and other studies into perspective, we discuss and advocate procedures for reproducible and meaningful experiments. Thus, we identify best practice in both



Steven E. F. Kleijn received his BSc from Leiden University and Delft University of Technology (The Netherlands), and his MSc in Chemistry from Leiden University and partially Osaka University (Japan) in 2009. He then carried out PhD research on electrocatalysis at single nanoparticles at Leiden University and the University of Warwick.



Marc T. M. Koper studied Chemistry at Utrecht University, The Netherlands, and completed his PhD (1994) there with Prof. J. H. Sluyters. After postdoctoral research at the University of Ulm (Germany) (EU Marie Curie Fellowship) and at Eindhoven University of Technology (Royal Netherlands Academy of Arts and Sciences), he became Professor in Fundamental Surface Science at Leiden University in 2005. His research interests are in fundamental studies of electrochemical and electrocatalytic processes through a combination of experimental and theoretical investigations.



Stanley C. S. Lai received his MSc in Chemistry from Leiden University (The Netherlands) in 2006 and obtained his PhD with Prof. Marc Koper on the electrocatalytic oxidation of ethanol from Leiden University in 2010. After postdoctoral research (EU Marie Curie Fellowship) at the University of Warwick (UK), he moved to the University of Twente (The Netherlands) in September 2013. His research interests concern electrocatalytic materials and reactions using a combination of electrochemical, spectroscopic, and high-resolution imaging techniques.



Patrick R. Unwin joined the University of Warwick in 1992 and has been Professor of Chemistry since 1998. He received his BSc (Leverhulme Prize and Leblanc Medal) from the University of Liverpool in 1985 and PhD from the University of Oxford in 1989, where he was Dee Graduate Scholar at St. Hugh's College and Junior Research Fellow in Physical Science at Balliol College. From 1990 to 1991, he was a NATO Fellow at the University of Texas at Austin. His interests are in new methods for investigating interfacial processes, with a major focus on high-resolution multifunctional imaging techniques.



highly defined nanoparticulate electrocatalysis and the electrochemistry of single NPs.

The structure of this Review is as follows. First, we briefly outline a number of important and commonly studied reactions in electrocatalysis that are referred to throughout the Review, highlighting the present status and outstanding issues. We then discuss common synthesis methods for NPs and procedures for obtaining reproducible electrocatalysis measurements. This is followed by an assessment of recent results from electrocatalytic measurements on ensembles of NPs, where there is a high degree of control over particle shape or mass-transport conditions. These model studies in many ways represent the recently established state-of-the-art. Finally, we give detailed attention to emerging innovative techniques that are able to target single NPs, and in the best cases relate structure and activity at a single NP. The Review concludes by summarizing the main issues and by providing an outlook for the further development of this important field.

### 1.1. Important Reactions

Fuel-cell reactions are among the most studied electrocatalytic reactions, and we will frequently make reference to them. It is thus useful to give some background on selected reactions to indicate critical issues involved in respect to electrocatalysis and the relationship of activity to the properties of NPs.

#### Oxygen Reduction Reaction (ORR)

The electroreduction of oxygen is critical to the efficiency of (hydrogen) fuel cells<sup>[39]</sup> and metal–air batteries.<sup>[40,41]</sup> The thermodynamic equilibrium potential for the ORR is 1.23 V versus the reversible hydrogen electrode (RHE), but even on the most active catalyst materials (Pt group metals) significant current is only measured at potentials below 0.9 V.<sup>[42]</sup> Recent theoretical studies have provided new insights into the origins of the slow ORR kinetics:<sup>[28,43]</sup> the binding energy of several oxygen-containing intermediates with the electrode surface is key, and platinum surfaces appear to provide interaction energies close to the theoretical optimum.

The full reduction of oxygen to water entails the transfer of four electrons in steps that are depicted schematically in Figure 2. The present view is that the predominant mechanism involves an adsorbed hydrogen peroxide intermediate that may convert and desorb as  $\text{H}_2\text{O}_2$ , before undergoing further reduction. The formation of hydrogen peroxide is undesired as it reduces the effective cathodic current, contaminates the surroundings of the catalyst, and corrodes the polymer membrane present in fuel cells. Pt is the best monometallic electrode material for the ORR because the oxygen–oxygen bond can be broken on Pt surfaces, with relatively little interference from the formation of an irreversible oxide. In contrast, on very noble metals such as Au, the ORR does not proceed appreciably beyond the reduction to hydrogen peroxide. Transition metals, on the

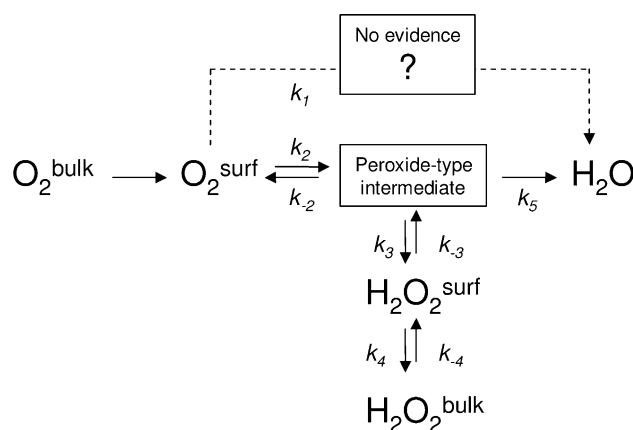


**Figure 2.** A proposed mechanism for the oxygen reduction reaction (ORR).

other hand, are prone to form stable oxides, thereby leaving the dissociated oxygen immobilized.<sup>[43]</sup>

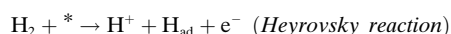
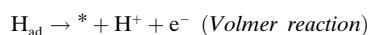
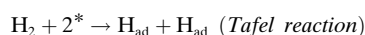
The structure sensitivity of the ORR on Pt has been investigated through the use of single-crystal electrodes. The structural sensitivity of the ORR in sulfuric and phosphoric acid solutions mirrors the relative adsorption strength of the electrolyte anions, which adsorb most strongly on the (111) surface and which concomitantly shows the lowest ORR activity.<sup>[44]</sup> Anion adsorption does not occur in perchloric acid solutions, and the ORR activity is significantly increased.<sup>[44]</sup> A detailed study of single crystals with various terrace lengths has shown that ORR activity increases with increasing step density (i.e. decreasing terrace width). Infinite (111) terraces show the lowest activity,<sup>[45]</sup> but the absolute difference in activity between different crystal structures is much less pronounced than in sulfuric acid. Although studies of this type provide valuable fundamental information, the projection of these findings to predict the effects of NP shape and size on the ORR is not straightforward.

In terms of NP studies, a prevalent view has been that the ORR activity decreases as the NP size decreases.<sup>[5,30]</sup> This has been rationalized by the suggestion that the main contribution to the ORR comes from the fraction of extended terraces on NPs, which is increased with larger NPs.<sup>[46]</sup> However, this view opposes the experimental findings on single crystals outlined above,<sup>[45]</sup> thus highlighting the difficulty of translating information between NP studies and macroscale measurements for the ORR. Watanabe et al. have argued that apparent NP size effects on ORR activity can be influenced by experimental design, and, particularly, diminished mass transport to individual NPs in an ensemble as the particle loading increases.<sup>[47]</sup> Recent findings concerning high NP loadings on a support indicate that hydrogen peroxide generated at an NP may readsorb on neighboring NPs and thereby improve the overall ORR yield.<sup>[48]</sup>

The influence of both NP size and diffusion effects on the ORR are important topics of debate, and we will discuss herein recent efforts to study this reaction at individual NPs (Section 5), as well as at NP ensembles under conditions of well-controlled mass transport (Section 3).

## Hydrogen Evolution Reaction/Hydrogen Oxidation Reaction

The hydrogen oxidation reaction (HOR) is the fuel-consuming reaction in fuel cells and the hydrogen evolution reaction (HER) is the cathodic reaction in electrolyzers used to produce hydrogen. Both reactions are characterized by extremely fast kinetics on platinum electrodes<sup>[49]</sup> and almost perfect reversibility (particularly compared to the complete lack of reversibility of the oxygen reduction and evolution reaction). Although the best catalyst for both reactions, Pt, has been known for centuries, materials research to improve the HER/HOR focuses on reducing or removing the Pt content altogether, or on modifying Pt to increase resilience towards carbon monoxide.<sup>[50–52]</sup> Carbon monoxide is a common feedstock contaminant in H<sub>2</sub> produced by steam reforming of hydrocarbons. The following steps describe the HOR:<sup>[30]</sup>



where \* indicates a vacant site at the catalyst surface. Definitive determinations of the mechanism and NP size-dependence have remained elusive because of the complications posed by the fast kinetics of the HOR.

The counterpart HER reaction is not hindered by mass transport in the high-proton concentrations of acidic electrolytes relevant for electrolyzers. On the macroscale, the Pt(110) surface is the most active,<sup>[44]</sup> while HER activity has been observed to increase as the particle size decreases,<sup>[53,54]</sup> as discussed in more detail in Section 5.1. It is well established that the HER on Pt follows a Volmer–Tafel mechanism.<sup>[30]</sup>

## Hydrazine Oxidation

Hydrazine (N<sub>2</sub>H<sub>4</sub>) is a potent fuel that can be oxidized to form molecular nitrogen and water in a four-electron reaction. The reaction proceeds very rapidly through successive deprotonation steps that leave the N–N bond intact.<sup>[55,56]</sup> On Au there is an overpotential of almost 500 mV with respect to Pt,<sup>[56]</sup> but, for both metals, once the onset potential is reached, a mass-transport-limited situation is readily established on further increasing the potential. Carbon electrode materials are essentially completely inactive towards hydrazine oxidation. As a result of this strong dependence of the onset potential on the type of electrode material, as well as the fast reaction kinetics, hydrazine oxidation has proven highly suitable to distinguish between different electrode materials, thus making it a good redox probe for the NP collision experiments that are discussed in Section 5.2.

## 2. Preparation and Characterization of Nanoparticulate Electrocatalysts

A key aspect to the study and employment of NPs as electrocatalysts is the preparation and characterization of nanoparticulate electrodes, which often consist of NPs dispersed on a (typically non-electrocatalytic) support material. In such electrodes, the NP support plays a number of roles. First and foremost, from a practical point of view, the support electrode acts as a conductive bridge, contacting the NPs to an external electronic circuit. Second, the support acts to disperse the NPs, to limit agglomeration, and maintain the high surface-to-volume ratio desired. Finally, the interaction between the support material and the NPs can be employed to modify the electrocatalytic activity of the NPs.<sup>[57]</sup> For example, Hayden et al. showed that titania-supported Au NPs have a higher activity for the electrochemical oxidation of CO than carbon-supported Au NPs,<sup>[57]</sup> while titania-supported Pt NPs are less active for CO oxidation<sup>[58]</sup> and oxygen reduction<sup>[59]</sup> than carbon-supported Pt NPs. Although the occurrence of such support effects is well-known in gas-phase heterogeneous catalysis,<sup>[60–63]</sup> the interplay between the support material and NP activity is significantly less understood in electrocatalysis.

The most common support materials are various types of carbon,<sup>[64–68]</sup> as the electrodes used in fuel cells are typically carbon-based. In addition, carbon is cheap and relatively inert towards many electrocatalytic (bond-breaking and bond-making) processes. For fundamental studies, gold has found considerable use as it can be cleaned and characterized easily, and provides a stable surface.<sup>[69,70]</sup> Titania has also received attention as a model in studies of support effects,<sup>[57,59]</sup> while doped tin oxides are typically employed as support materials for applications where optically transparent electrodes are desirable.<sup>[71–73]</sup>

While there are numerous methods to prepare and immobilize NPs on conductive supports, they broadly fall into three categories (Figure 3): a) simultaneous (single-step) formation and immobilization of NPs; b) immobilization of metal ions followed by their reduction to metal NPs; c) synthesis of metal NPs followed by their immobilization on the surface of the support electrode.

### 2.1. Single-Step Nanoparticle Formation and Immobilization

In this approach, the formation and immobilization of NPs on a support electrode takes place in a single step. Examples of this approach are: the electrodeposition of NPs from a solution containing the metal ion, either onto the bare support electrode<sup>[74–82]</sup> or onto the support electrode modified with a polymer film,<sup>[78,83–86]</sup> electroless deposition,<sup>[77,87,88]</sup> and vacuum evaporation.<sup>[89–93]</sup> Electrodeposition is by far the most popular of these methods, as it makes use of electrochemical equipment, ensures an electrical contact between the NP and substrate, and provides many tunable parameters, such as the deposition potential or current, time, temperature, and electrolyte composition,<sup>[74,75,94]</sup> to adjust the size, shape, and spatial distribution of the electrodeposited NPs. The coupling

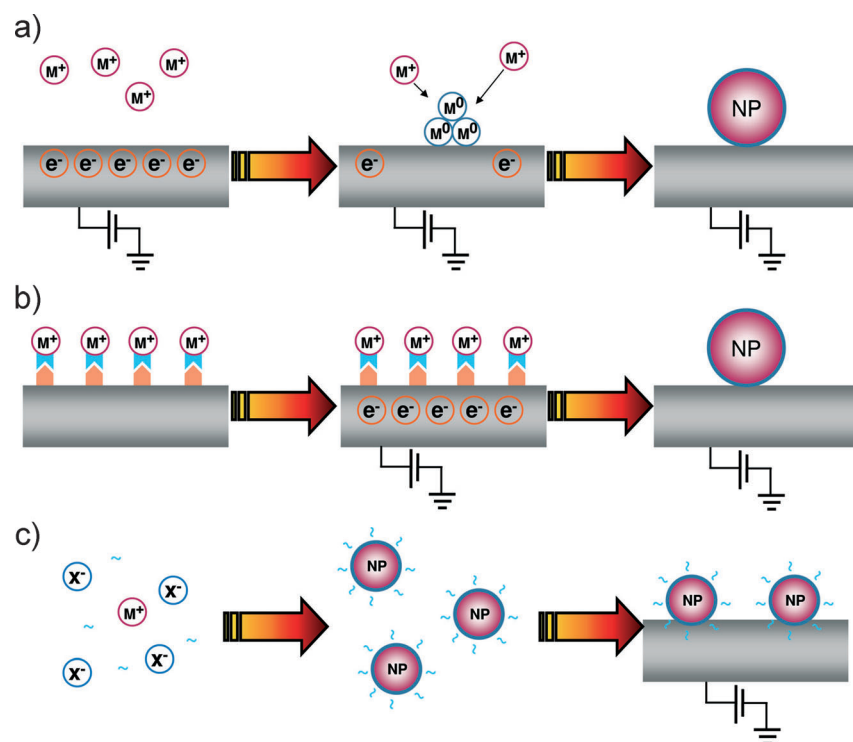


**Figure 3.** Three general approaches to fabricate a nanoparticulate electrode: a) simultaneous NP formation and immobilization; b) immobilization of metal ions followed by reduction; c) synthesis of metal NPs followed by their immobilization.

of electrodeposition experiments with other characterization techniques, such as *ex situ*<sup>[95–97]</sup> and *in situ* TEM,<sup>[98,99]</sup> as well as small-angle X-ray scattering (SAXS)<sup>[100]</sup> has provided valuable insights into the early stage of NP formation, which may ultimately lead to improved electrodeposition procedures.

The main drawback of electrodeposition, at present, is that it typically leads to NP deposits with a wide size distribution.<sup>[74]</sup> There are three reasons for this. First, new NP nuclei (small clusters of atoms) may form during the entire duration of the electrodeposition process (progressive nucleation).<sup>[74,76]</sup> This leads to a wide distribution in growth time for individual NPs, and, consequently, in NP sizes. Second, during growth, depletion layers of neighboring NPs can start to overlap, causing these NPs to grow more slowly compared to those which are diffusionally isolated.<sup>[101]</sup> Consequently, the size of a single NP correlates with the local number density of NPs. As the number of nearby NPs will vary from one NP to the next in a random ensemble, this leads to a broadening of the size distribution during NP growth.<sup>[101]</sup> Third, (surface-mediated) Ostwald ripening can occur, whereby large NPs grow at the expense of the small NPs because of the size-dependence of the free energy of stabilization of an NP.<sup>[102,103]</sup>

To circumvent the size dispersion as a result of the progressive formation of new nuclei, efforts have been made to separate, in time, the formation of nuclei and the growth of those nuclei. This control is typically achieved by forming nuclei with a short (< 10 ms) potential pulse at high overpotential with respect to the reduction potential of the metal

ions in solution, followed by a long growth pulse (up to a few minutes) at low overpotential, where no new nuclei are formed and all growth occurs on preformed nuclei.<sup>[71,74,75,77,104–109]</sup> Slow NP growth at low overpotential also diminishes the concentration polarization near the substrate, so that local NP coverage has less effect on the extent of growth of individual NPs. This double potential pulse approach has been successfully employed to electrodeposit reasonably monodisperse NP arrays of various metals.<sup>[71,74,75,77,104–109]</sup>

Depletion effects can also be minimized by incorporating a local source of convection within the depletion layer. An easy way to achieve this is to drive a gas-evolving reaction (in practice through the coevolution of hydrogen from protons) in parallel with the electrodeposition reaction, so that the formation and release of gas bubbles drive convective mixing near the growing NP.<sup>[110,111]</sup> Although H<sub>2</sub> coevolution leads to the size distribution narrowing,<sup>[110]</sup> the resulting NPs are typically nanocrystalline and fractal in nature.<sup>[110,111]</sup> Finally, the deposition of NPs in a periodic array ensures that mass transport to each NP is similar.<sup>[112]</sup> However, this method is rarely employed, as it involves extensive pretreatment of the substrate electrode to create a periodic array of nucleation sites.

## 2.2. Immobilization of Metal Ions Followed by Reduction

In this two-step procedure, metal ions are immobilized on the electrode surface before being reduced (either chemically or electrochemically) to form NPs directly attached to the surface. The spatial distribution and average size of the resulting NPs are determined by the amount of metal precursor, which can be controlled by adjusting the density of metal ion immobilization sites. By limiting the amount of immobilized ions, the preparation of small NPs is facilitated.

A key challenge of this approach is the controlled introduction of functional groups that coordinate to the desired metal precursor on the electrode surface. One option is to immobilize ions within a polyelectrolyte film deposited onto the substrate electrode,<sup>[113–118]</sup> thereby leading to the encapsulation of NPs within the polyelectrolyte film. Although this encapsulation provides a steric barrier to particle agglomeration, the resulting NPs may be less catalytically active than bare NPs.<sup>[113]</sup> An alternative method to functionalize the support electrode is diazonium coupling,<sup>[119–123]</sup> which can be performed on many electrode surfaces (metal, semiconductor, carbon), but is most commonly employed on carbon electrodes (such as highly oriented pyrolytic graphite (HOPG)<sup>[107]</sup> and carbon nanotubes).<sup>[124–126]</sup>

### 2.3. Synthesis of Metal Nanoparticles Followed by Immobilization

Optimal control of NP size and shape can be achieved by separating NP formation from the immobilization step, by synthesizing NPs in solution and then attaching the NPs to the support electrode. NPs are most often prepared in solution by colloidal synthesis, an empirical method which offers excellent shape and size control, and requires simple equipment. A rich body of literature has developed since the seminal work by Turkevich et al.,<sup>[127]</sup> followed up by Brust, Bethell, Schiffrin, and co-workers.<sup>[128]</sup> The principle of colloidal synthesis is straightforward and, in general terms, three components are required for the synthesis: a metal precursor (metal salt) which provides the metal ions, a reducing agent (such as  $H_2$ ,  $BH_4^-$ , or citrate) which reduces the metal ions to metal atoms to form NPs, and a stabilizing agent (such as citrate or various polymers) which limits the size and prevents the NPs from agglomerating. Solutions of the three chemicals are mixed together, causing the formation of metal nuclei, which grow by the addition of atoms.<sup>[129]</sup> The equilibrium shape of an NP, as predicted by the Wulff theorem, is a polyhedron and, at a larger radius, a sphere.<sup>[130]</sup> The final morphology of the particle can be altered by controlling the kinetics of the growth, for example, by adding surfactants that bind preferentially to specific surface facets, thereby slowing their growth rate.<sup>[131,132]</sup> Controlling the conditions allows the tailored synthesis of shape-selected NPs, with specific surface facets exposed, which is beneficial to the catalysis of selected reactions (see Section 4).<sup>[35,131–133]</sup>

The colloidal synthesis of dendrimer-encapsulated NPs is an interesting approach that brings additional control options.<sup>[67,134–140]</sup> Dendrimers are hyperbranched, highly regular macromolecules, consisting of a central core from which branched (monomer) units extend.<sup>[141,142]</sup> In this approach, metal ions are trapped at functional groups within the well-defined dendrimers before being reduced to the corresponding metal NPs. Conceptually, this is similar to the ion-immobilization/reduction approach described above, with the main difference being that the dendrimer is in solution rather than tethered on the electrode surface. Dendrimers are attractive for the synthesis of NPs for a number of reasons: 1) The dendrimer templates can be synthesized with a high degree of control by defining the number of generations (number of “layers” of monomer units) in the dendrimer synthesis, and thus the number of ion-anchoring functional groups can be controlled. This allows NPs to be synthesized from less than 1 nm up to 4–5 nm with a relatively narrow size distribution through the number ion-anchoring groups.<sup>[67,134–140]</sup> 2) The NPs are encapsulated within the dendrimers, which serve as stabilizing agents to prevent agglomeration. 3) The open dendrimer structure and the fact that NP stabilization is mainly due to steric effects leave a significant fraction of the NP surface available for catalytic reactions. 4) The dendrimer branches can be functionalized to act as selective gates to the NPs. 5) The terminal groups on the exterior of the dendrimer branches can be modified to control the solubility of the dendrimer-encapsulated NP or to tether it to electrode surfaces.<sup>[143]</sup>

A novel method of NP fabrication has recently been reported under the name “cathodic corrosion”. In this electrochemical method, Yanson et al. demonstrated that NPs of various metals (Pt, Au, Cu, Ag, Ni, Rh, Si, Nb, and Ru) and metal alloys (PtRu, PtIr, PtNi, AuCo, AuCu, and FeCo) can be formed from pristine metal wires by simply applying a very negative potential of about  $-5$  or  $-10$  V to the metal in an aqueous electrolyte containing a strong nonreducible cation, hence the name “cathodic corrosion”.<sup>[144,145]</sup> Application of an alternating voltage aids in dispersing the NPs, but is not essential to their formation. Furthermore, it was shown by tuning the electrolyte concentration and the electrical current that the shape and size of the NPs could be controlled.<sup>[146,147]</sup> A major advantage of this method is that it offers a similar degree of shape and size control as the colloidal synthesis of NPs, but does not require a stabilizing agent or other additives during the synthesis, thus leaving the NPs clean. Furthermore, this method is versatile, as it allows the fabrication of NPs of almost any metal and metal alloy.

To employ synthesized NPs for electrochemical studies, one needs to immobilize them on the surface. Furthermore, some stabilizing agents on the NP surface may need to be removed to avoid interference with the NP reactivity. The most common method to attach solution-dispersed NPs to support electrodes is by simple drop-casting: an aliquot of an NP-containing solution is placed on the support electrode, and the solvent is left to evaporate, thereby leaving the NPs behind. Although straightforward, drop-casting often leads to inhomogeneous deposition with severe particle aggregation, particularly around the edges of the drops, similar to the “coffee-ring effect”.<sup>[148–150]</sup> Furthermore, the NPs are only weakly adhered to the surface through van der Waals forces, and NP detachment can be a significant problem.

An alternative way to tether NPs is to functionalize the support to provide specific anchoring sites for the NPs. This can be done by introducing a layer of functional groups onto the surface of the support electrode, through diazonium grafting (see previous section), or by functionalization with a self-assembled monolayer (SAM) which is terminated with a functional group that binds strongly to the NPs.<sup>[151–168]</sup> The formation of SAMs on surfaces is a broad research field that has been reviewed extensively.<sup>[169–173]</sup> SAMs are spontaneously formed monomolecular layers consisting of a head group that interacts with the surface, a molecular chain of variable length, and a terminating functional group. In the context of this Review, three main classes of SAMs should be considered, namely alkanethiols<sup>[162–168]</sup> and alkyl isocyanides<sup>[161]</sup> for (coinage) metal surfaces (such as gold electrodes), as well as alkoxysilanes for metal oxide surfaces (such as silica or doped tin oxide electrodes).<sup>[151–160]</sup>

To link to the NPs, the SAMs need to be terminated with a functional group that provides an anchoring site for the NPs. Typically, this functional group is a thiol,<sup>[151,159,160,162–164,174]</sup> amino,<sup>[151–156,159,167,168]</sup> or isocyanide<sup>[151,161]</sup> group, as these have a high affinity for metal NPs through the formation of covalent metal–sulfur or metal–nitrogen bonds, thereby displacing the stabilizing agent present on the NPs. An alternative method of tethering NPs is to imbue a charge, typically by depositing a charged polymer (polyelectrolyte)



on the support surface with a charge opposite to that of the NPs, thereby binding the NPs electrostatically.<sup>[157,165,166,175]</sup> By tethering the NPs to the surface through a linker molecule, a more uniform surface distribution with minimal agglomeration can be obtained,<sup>[157,175]</sup> as the binding sites to the NPs are regularly arranged in a quasi-two-dimensional plane.

When using the tethered NPs as electrocatalysts, it is imperative that electron transfer (ET) can occur across the SAM between the NP and the underlying substrate. Classically, in the absence of NPs, ET across an insulating layer is determined by the probability of electron tunneling through the layer. This probability is proportional to  $\exp(-\beta d)$ , where  $\beta$  is the tunneling decay constant ( $\beta \approx 1 \text{ \AA}^{-1}$  for saturated hydrocarbon bridges)<sup>[165–167,176–179]</sup> and  $d$  is the thickness of the insulating layer. Practically, this exponential decay means that hydrocarbon-based SAMs (such as alkanethiols) with chains longer than about 10 carbon atoms would essentially completely block ET between species in solution and the electrode surface, and no Faradaic electrochemistry from the redox species in solution would be observed, as has been amply demonstrated.<sup>[157,159,165–167,174,180,181]</sup> Interestingly, the adsorption of NPs on top of the SAM opens up a pathway for ET across the SAM, which was found to be as efficient as in the absence of a SAM.<sup>[157,159,165–167,174,180,181]</sup> The research groups of Fermín<sup>[165,166,182]</sup> and Gooding<sup>[167,174,180]</sup> have shown in a series of systematic studies that NP-mediated ET appears to be relatively distance-independent (i.e.  $\beta \approx 0$ ) for typical SAM layers and, furthermore, that ET between the redox species and the NP is the rate-limiting step (rather than ET across the layer).

These findings have been rationalized in a theoretical description of NP-mediated ET by Chazalviel and Allongue.<sup>[183]</sup> This theory considers ET between: 1) a redox couple and a metal electrode (represented by the exchange current density  $J_0$ ) and 2) a metal NP and a metal electrode (represented by the exchange current density  $J_1$ ; Figure 4a). Typically,  $J_1$  is about twelve orders of magnitude larger than  $J_0$ , unless an NP is particularly small.<sup>[183]</sup> The introduction of an insulating layer, such as a SAM on the electrode, causes a decrease in the ET rate proportional to  $\exp(-\beta d)$  (see above). Typically,  $J_1$  is sufficiently large that even  $J_1 \exp(-\beta d)$  is still much larger than  $J_0$ , and the adsorption of NPs thus opens up an effective ET pathway across the SAM. An important consequence of this model is that NP-mediated ET is unimpeded by the presence of a SAM as long as the NP is relatively large compared to the thickness of the layer (Figure 4b), a prediction which has been validated experimentally by Gooding and co-workers (Figure 4c).<sup>[180]</sup>

Importantly, for NPs tethered to an electrode surface through a SAM, the Chazalviel–Allongue theory<sup>[183]</sup> demonstrates that ET across the SAM is only impeded in the case where the NPs are very small (and very monodisperse, as a few NPs above the critical size could already provide an efficient ET pathway) or the SAM is rather thick. Otherwise, NP tethering is an efficient way to immobilize NPs on a support electrode with minimal NP aggregation or desorption, which can also be applied to study electrocatalytic processes.<sup>[157]</sup>

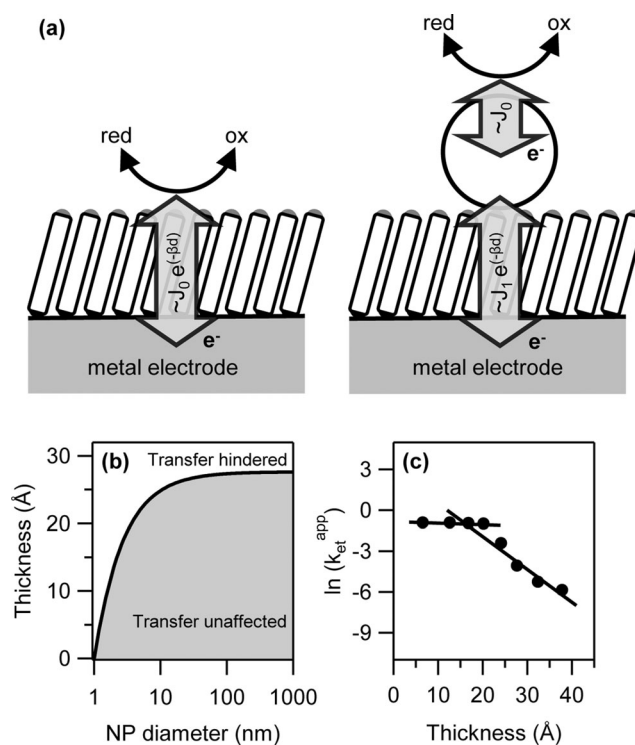


**Figure 4.** a) Comparison of electron transfer between a redox couple and a support electrode across a SAM (left) and nanoparticle-mediated electron transfer (right). Adapted from Ref. [183]. 2011, American Chemical Society. b) Theoretical prediction of the critical thickness of an insulating layer (between a collector electrode and a metal NP), which leads to a change in the voltammogram of a reversible system in solution compared to a bare metal electrode (adapted from Ref. [183]). c) Variation in the apparent electron-transfer kinetic constant for the one-electron reduction of  $[\text{Ru}(\text{NH}_3)_6]^{3+}$  to  $[\text{Ru}(\text{NH}_3)_6]^{2+}$  on 27 nm AuNPs with the thickness of an insulating poly(ethylenediamine) layer. Adapted from Ref. [180]. 2012, American Chemical Society.

## 2.4. Cleaning

When a nanoparticulate catalyst is prepared through surfactant-free techniques such as vacuum deposition, electrodeposition, electroless deposition, or cathodic corrosion, additional cleaning steps are often not required. Colloidal NPs, however, necessarily have a layer of surfactant molecules on their surface. Since this surfactant film could inhibit the adsorption of reactants in catalytic reactions,<sup>[184]</sup> it needs to be removed as part of the catalyst preparation.

Solla-Gullón et al. demonstrated the use of CO adsorption on surfactant-coated Pt NPs as a method for cleaning NPs.<sup>[185]</sup> Since CO adsorbs preferentially on Pt, the surfactant is displaced by a monolayer of CO, which can then be stripped off the surface electrocatalytically in a subsequent oxidative potential sweep. The cleanliness of the surface can then be assessed through electrochemical characterization of the NPs, as discussed below. Although CO gas should be handled with caution, this method is very successful at cleaning NP surfaces and can be applied to all metals that adsorb CO strongly, for example, for the cleaning of Pt<sup>[185]</sup> and Pd NPs.<sup>[186]</sup>

An alternative cleaning method was reported by Rodriguez and Koper,<sup>[187]</sup> who showed that the surface of Pt NPs



capped with polyvinylpyrrolidone (PVP) can also be cleaned with a dilute sulfuric acid solution containing  $\text{H}_2\text{O}_2$ , thereby leaving a clean Pt surface (as characterized electrochemically). Importantly, it was found that this method leaves the superficial order of the NPs intact. It was suggested that the decomposition of hydrogen peroxide on the Pt surface creates oxygen gas bubbles at the NP surface that physically displace the PVP molecules.

The Feliu research group have studied the effect on the NP surface structure of cleaning catalyst layers by using UV/ozone treatment,<sup>[188]</sup> as this was reported by Somorjai and co-workers to increase the catalytic activity of colloidal particles in gas-phase catalysis.<sup>[189]</sup> Through voltammetric analysis, it was found that ozone treatment actually severely perturbs the original surface structure of the NPs, in a way similar to the changes in the surface structure resulting from electrochemical adsorption of oxygen.

## 2.5. Characterization

After surface adsorbates have been removed from NPs, it is important to determine the NP shape and size as well as the total NP surface area exposed to the electrolyte. These characteristics can be determined by a combination of techniques that can be roughly divided into electrochemical and non-electrochemical methods.

### Electrochemical Characterization

A very accurate way to determine both the exposed surface area and the dominant surface structure of noble metal electrodes is through the study of adsorbed monolayers of atomic or molecular fragments. Examples are the under-potential adsorption and desorption of hydrogen on Pt surfaces ( $\text{H}_{\text{UPD}}$ ) and the formation of oxide monolayers.<sup>[190,191]</sup> The number of surface atoms exposed to the electrolyte, or the electrochemically active surface area,<sup>[192]</sup> can be determined from the charge passed during the adsorption or desorption of a monolayer. Moreover, the voltammetric signature for monolayer formation or monolayer “stripping” can be very sensitive to the surface structure, as has been shown for hydrogen adsorption/desorption on Pt single-crystal electrodes.<sup>[190]</sup> When this is applied to nanoparticulate electrodes, an average NP shape can be deduced from the relative number of surface facets measured by using such techniques (Figure 5).

Analysis of the shape and surface structure of Pt NPs through electrochemical characterization has been extensively developed by Feliu and co-workers.<sup>[70,193]</sup> Site-specific irreversible adsorption of adatoms was employed to identify the ratio of the various exposed surface facets on shape-selected Pt NPs. Specifically, it was shown that bismuth and tellurium adsorb selectively on (111) terraces with widths of more than three atoms, while germanium adsorbs selectively on (100) terrace sites. After adsorption, these adatoms can be stripped, thereby revealing quantitatively the amount of adsorption, and hence values for the amount of each surface. The relative fractions of (111) and (100) sites were deter-

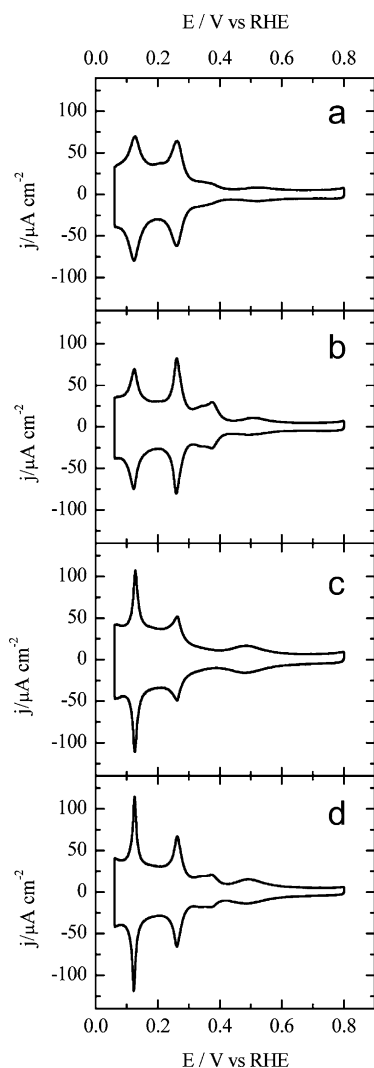


**Figure 5.** Cyclic voltammograms corresponding to a) spherical (polyoriented) Pt NPs, b) cubic Pt NPs (rich in (100)-type sites), c) octahedral and tetrahedral Pt NPs (rich in (111)-type sites), and d) truncated octahedral and tetrahedral Pt NPs (rich in (111)-type and (100)-type sites) in 0.5 M  $\text{H}_2\text{SO}_4$  ( $50 \text{ mVs}^{-1}$ ). The voltammogram shows different features related to different types of sites: peak at 0.125 V for (110)-type sites, peak at 0.27 V containing contributions from (100) step sites on (111) terraces and sites close to steps on the (100) terrace, broad peak at 0.35–0.37 V for (100) terraces, and a broad peak at 0.5 V related to (111) terraces. Adapted from Ref. [193]. 2012, American Chemical Society.

mined for NPs of various shapes by this method, and found to be in agreement with the analysis of the shape of NPs obtained by TEM measurements.<sup>[70]</sup> Recently, the same research group reported a detailed characterization of the surface domains on Pt NPs by careful measurement of the hydrogen adsorption and desorption region, as well as the oxidation of CO, in sulfuric acid, perchloric acid, and sodium hydroxide electrolytes.<sup>[193]</sup>

There are fewer reports on the electrochemical characterization of NPs formed from metals other than Pt, although some methods are noteworthy. The voltammetry of Pd in sulfuric acid also exhibits electrochemical signals corresponding to the adsorption and desorption of monolayers of oxide

and hydrogen, which can be used for structure-sensitive determination, and this has been used to characterize Pd NPs.<sup>[186]</sup> The electrochemical determination of the surface structure of Au NPs has been achieved by the underpotential deposition (UPD) of Pb.<sup>[194]</sup> The voltammetric signal of Pb UPD is surface-sensitive and shows contributions from the three Au basal planes. Nanoparticulate Ru electrodes can be characterized using CO stripping and Cu UPD.<sup>[195]</sup> In general, CO stripping can be used to determine the electrochemically active surface area of a range of metal NPs.<sup>[196–199]</sup>

### Non-Electrochemical Characterization

The size and/or shape of NPs can be evaluated through several techniques. Atomic force microscopy (AFM) and X-ray diffraction (XRD) can be used relatively easily to estimate NP size. AFM is a scanning probe technique that is highly sensitive to height changes out of the plane.<sup>[200]</sup> However, its lateral sensitivity is not sufficient to detect the shape of (small) NPs, but the height change with respect to the plane can be taken as the diameter of an NP.<sup>[200]</sup>

The width of the diffraction peaks in XRD is related to the size of the average crystallite in the sample under study, and in the case of (small) NPs it can be assumed that each NP consists of a single crystallite and the NP diameter can then be determined from the well-known Scherrer Equation.<sup>[201]</sup> It should be noted that the Scherrer Equation depends on the crystallite shape (e.g. spherical or cubic), so that high-precision size measurements can only be made by XRD when another microscopic technique is used to determine the NP shape.<sup>[201]</sup> Since the Scherrer Equation yields the average crystallite size, XRD is not a good means to estimate the dispersion of NP sizes.

The rapid size determination of NPs with a large photon scattering cross-section can be achieved by a number of optical methods, such as dynamic light scattering (DLS)<sup>[202]</sup> and NP-tracking analysis (NTA).<sup>[203]</sup> In DLS, a laser beam is shone through a dilute solution of colloidal NPs, and the light transmission is measured as a function of time. The NPs in solution act as point scatterers. Brownian motion causes the NPs to move in solution, thus causing the interparticle distance to change and giving rise to either constructive or destructive interference of the scattered light by surrounding NPs. This causes fluctuations in the transmission. The time-scale of these fluctuations can then be correlated with the timescale of the movement of the NPs. The diffusion coefficient and NP size can be determined through Equation (3) (Section 5.2). It should be kept in mind that this analysis is complex, especially for a polydisperse sample.

Similar to DLS, NTA exploits the fact that NPs in solution act as point scatterers.<sup>[203]</sup> However, rather than inferring the motion of NPs from the overall intensity of the transmitted light through an NP solution, NTA follows the Brownian motion of NPs directly in real time. This is done by mounting the cell containing a solution of NPs onto an optical microscope equipped with a high-speed CCD camera, which allows the visualization of the position of individual scatterers (NPs) when a laser beam is passed through the sample. By following the position of many NPs separately over time (typically less

than a minute), the average distance moved by individual NPs is calculated, and the size of each individual NP is derived to construct a size distribution.

Importantly, both DLS and NTA rely on measuring the intensity of scattered light, which for NPs much smaller than the wavelength of the incident light can be described by Rayleigh scattering.<sup>[204]</sup> The scattering cross-section is dependent on the refractive index of the material and very strongly dependent on NP size, which limits the applicability of light-scattering-based techniques to the characterization of relatively large NPs (> 10 nm) made from highly refractive materials, such as gold, silver, and, to a lesser extent, other metals.<sup>[204]</sup>

Finally, UV/Vis absorption spectroscopy can be employed for the size determination of NPs of metals for which the wavelength of absorbed light depends strongly on the particle size. In practice, this method is mostly limited to Au and Ag NPs.<sup>[205,206]</sup>

Transmission electron microscopy (TEM) measurements are required to judge the particle size with certainty and visualize the average particle shapes obtained in the synthesis. No other measurement technique gives the accuracy level of TEM, which, in modern, high-resolution versions, even allows for the determination of the exposed crystal-surface facets of a particle.<sup>[207]</sup> Interestingly, the use of high-resolution TEM combined with electron tomography can accurately image single NPs as well as NP clusters and has helped in elucidating the growth mechanism of electrodeposited NPs.<sup>[208]</sup>

## 3. Model Approaches to Real Catalysts

As has been pointed out in the Introduction, it is extremely difficult to extract even the intrinsic (average) activity of NPs from measurements on real catalysts (Figure 1a). In this section we discuss approaches that have been developed to mimic the mass-transport conditions of fuel-cell electrodes and study the influence of mass transport on catalyst performance in model systems. In ideal situations, such experiments use NPs of very well defined size and/or interparticle distance. Moreover, the use of flow cells offers a high degree of control over the mass transport of reactants to arrays of NPs. These measurements thus allow the accurate evaluation of important catalyst parameters such as the effect of particle size or of catalyst loading on rates and reaction pathways.

### 3.1. Influence of Mass Transport

The nature of mass transport towards a nanoparticulate electrode is indicated schematically in Figure 6. When the support material is inert, a radial concentration gradient forms around the NPs performing the electrocatalytic reaction, thus creating “diffusion spheres”. The distance from the electrode where the concentration is 90 % of the bulk concentration (or, technically, 90 % of the bulk concentration minus the surface concentration) can be considered as the thickness of the diffusion sphere. Overlap between the

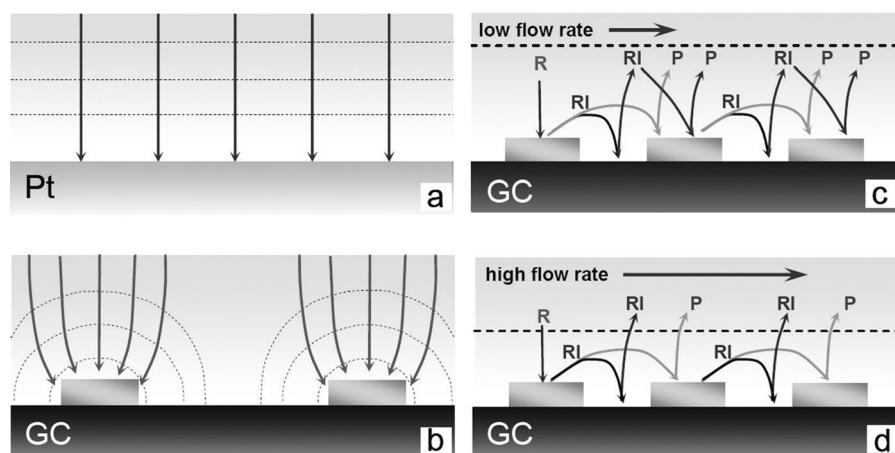


**Figure 6.** Mass transport towards electrodes: diffusion towards an infinite planar electrode is linear (a), while well-separated NPs show radial diffusion spheres (b). As the inter-NP distance is decreased, the diffusion spheres start to overlap. In (c) and (d), the influence of flow rate on mass transport to a NP array is illustrated: at low flow-rate, the diffusion layer is large and there is a chance for reaction intermediates (RIs) generated at an NP to readsorb on adjacent NPs (c). When the flow rate is increased, the diffusion layer effectively becomes thinner and RIs are less likely to readsorb, thus escaping from the NP ensemble (d). Adapted from Ref. [209]. 2010, The Electrochemical Society.

diffusion spheres leads to the formation of a continuous diffusion layer, and the electrode effectively acts as a planar electrode (Figure 6a).

Catalyst NPs in real devices experience rather complex mass-transport regimes that critically depend on the interparticle distance, which in turn depends on both the NP size and loading. As the inter-NP distance decreases, there is increasing diffusional overlap between adjacent particles in terms of both reactant diffusion and intermediate/product transport (Figure 6b). One particular impact on catalysis that has been seen in the ORR is that the diffusion-limited flux of oxygen to individual NPs in an array decreases and thus the apparent catalytic activity of each NP decreases.<sup>[47]</sup> The loading of NPs, and the impact on mass transport, is thus an important factor that needs to be accounted for when trying to compare intrinsic NP activities in different studies.

Behm, Kasemo, and co-workers have suggested that overlapping diffusion spheres may also enhance the overall catalytic activity for the ORR.<sup>[48]</sup> The mechanism of the ORR can proceed via hydrogen peroxide as an (adsorbed) intermediate (reaction  $k_3$  in Figure 2) and this species may desorb from the catalyst surface instead of reacting to give water, thus leaving the oxygen reduction incomplete. This aspect of the ORR is also considered below for measurements on individual Pt NPs (Section 5.1). If NPs are in proximity in an ensemble, there is an increased chance that the hydrogen peroxide produced on one NP will readsorb on an adjacent NP, and is reduced further to water, as illustrated in Figure 6c,d.<sup>[48]</sup> The chance that a reaction intermediate will readsorb depends on the degree of overlap of the diffusion zones of adjacent NPs. This diffusion sphere overlap can be predicted numerically<sup>[210,211]</sup> and also visualized using fluorescence confocal microscopy.<sup>[212]</sup>

It is thus apparent that studying the dependence of NP loading and interparticle distance for highly organized NP

arrays is hugely beneficial for uncovering any subtle influences of NP loading on electrocatalysis. Behm, Kasemo, and co-workers used lithographical techniques to fabricate an array of approximately 100 nm Pt disks on a carbon electrode, which was deployed as a working electrode in a flow-cell system, similar to the one shown in Figure 7.<sup>[213]</sup> The effect of the mass-transport rate could be investigated by: 1) varying the flow rate of the electrolyte over an ensemble of Pt nanodisks (Figure 6c,d) and 2) varying the radii and interparticle distance (Figure 6b). Increasing the flow rate (decreasing the diffusion layer thickness) or the interparticle distance serves to diminish diffusional coupling between neighboring NPs and thus reduces the chance of readsorption of RIs.<sup>[214]</sup> In this setup,

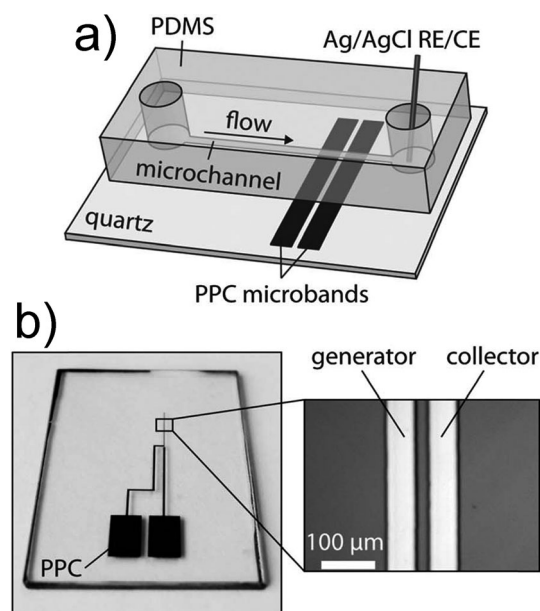


**Figure 7.** Electrolyte in a microchannel in PDMS (polydimethylsiloxane) flows across two pyrolyzed photoresist carbon (PPC) microband electrodes covered with dendrimer-encapsulated Pt NPs; the band closest to the flow source is the generator electrode, performing the ORR, and any residual products can be collected at the downstream collector electrode. RE: reference electrode; CE: counter electrode. Adapted from Ref. [216]. 2012, Royal Society of Chemistry.

a Pt electrode downstream of the Pt NP array was used to quantify the amount of hydrogen peroxide produced.<sup>[48]</sup> The amount of hydrogen peroxide detected downstream diminished as the NP density was increased and/or the flow rate was reduced (i.e. the mass-transport rate was reduced). The same effect was also demonstrated for other reactions that feature



soluble intermediates, such as the methanol oxidation reaction.<sup>[215]</sup>

The flow cell in Figure 7 was used by Dumitrescu and Crooks to study the effect of the flow rate on ensembles of well-defined dendrimer-encapsulated Pt NPs supported on microband electrodes.<sup>[216,217]</sup> A key attribute to this type of cell is that the hydrodynamics are very well defined and transport can be varied and controlled over a wide range.<sup>[214]</sup> Two working electrodes, each decorated with dendrimer-encapsulated Pt NPs, were placed adjacent to each other and perpendicular to the direction of electrolyte flow. The downstream electrode served as a “collector” electrode, and was held at a potential to oxidize hydrogen peroxide, while cyclic voltammetry was used to measure the ORR on the upstream “generator” electrode. It was found that the hydrogen peroxide yield (i.e. the fraction of H<sub>2</sub>O<sub>2</sub> formed relative to the total amount of O<sub>2</sub> consumed) remained constant even at elevated flow rates.<sup>[217]</sup>

A constant H<sub>2</sub>O<sub>2</sub> yield with flow rate was also observed by Behm and co-workers for extended polycrystalline Pt surfaces (see Figure 5c in reference [48]), consistent with the results of Dumitrescu and Crooks.<sup>[217]</sup> It should be noted that the dendrimer-encapsulated NPs were assumed to form a close-packed monolayer, which may be considered as a planar Pt electrode (Figure 6a). The relative yield of hydrogen peroxide during the ORR does not increase with increased flow rate (mass transport) over high-density planar Pt electrodes, but it does increase at increasing interparticle distance (i.e. lower catalyst loading).

### 3.2. High-Throughput Electrocatalyst Screening

Variations in the electrocatalytic activity with different NP sizes or NP loadings within an array can be screened particularly effectively using scanning electrochemical microscopy (SECM), a powerful technique for mapping the local reactivity.<sup>[218,219]</sup> A reactivity map is made while laterally scanning an ultra-microelectrode (UME; electrode with a critical dimension smaller than the diffusion layer thickness) in proximity to a larger electrode surface under study. Depending on the nature of the electrochemical reaction, the current is measured at the UME or at the substrate electrode. For example, the change in the ORR activity of an array of microdots containing Pd NPs with increasing Co content was mapped by generating oxygen at the scanning UME and measuring the ORR current of the electrode supporting the array.<sup>[220]</sup>

Many recent reports have appeared in which SECM was applied to assess a range of different material combinations for fuel-cell reactions,<sup>[221–224]</sup> as has been summarized in recent reviews.<sup>[219,225]</sup> While these studies identify appropriate procedures for measuring ORR activity, a careful study of catalyst activity as a function of catalyst loading (inter-NP distance) and NP size by SECM has not yet been performed. In light of the flow-cell studies described above, and others, such screening studies could be very interesting, considering the ongoing debate concerning the impact of NP size and loading on electrocatalytic activity (see Section 3.1). The use

of SECM to investigate electrocatalytic activity as a function of NP shape will be discussed in more detail in Section 4. It should also be noted that an interesting aspect of SECM is that the substrate does not need to be a biased electrode. One can use the tip UME to generate a reversible electron donor or electron acceptor that couples to an electrocatalytic reaction, thereby enabling studies of electrocatalytic NPs on an inert (insulating) support. This approach is thus valuable as a means for studying the effects of the support on ET at NPs. The approach has been used to study the HER at well-defined arrays of NPs in different environments.<sup>[226,227]</sup>

A particularly interesting method of model electrocatalyst screening has been reported by the research group of Hayden.<sup>[228]</sup> A masked substrate was used in an ultrahigh vacuum physical vapor deposition (PVD) chamber to deposit a range of different particle sizes in an array. Thin films of single metals or metal alloys (by simultaneously using multiple sources) could be deposited using a PVD source, and by imposing a shutter to partially shadow the source a range of deposition rates was obtained at different locations on the substrate.<sup>[229]</sup> Interestingly, if the deposited films were sufficiently thin, they formed nanoparticulate islands rather than a planar film. In this way, an array of different NP sizes could be easily generated, since the film thickness varied over the length of the substrate.<sup>[230]</sup> For these investigations, the substrate was an array of 100 planar microelectrodes (0.8 mm<sup>2</sup>) of ternary alloys (such as PdPtAu and TeGeSb) that were individually addressable, each with a different, but well-defined composition.

This approach was applied to the ORR at Pt NPs. The specific activity was shown to decrease sharply for NP sizes from 7 nm to 1 nm.<sup>[228]</sup> However, it should be noted that, with the PVD technique used, the distance between NPs decreased as the particle NP size was increased. Following on from some of the studies discussed above, the difficulty of controlling the interparticle distance and the mean NP size independently then makes it difficult to draw definitive conclusions about NP activity.

### 3.3. Stability of Nanoparticulate Catalysts

In terms of the application of NP catalysts, stability, as well as the activity and selectivity, is of paramount importance. Ideally, one would want to study structural changes of real catalysts during operation in a model environment, but in situ structural characterization is challenging. Although comparison of the electrochemical surface area before and after a measurement gives some insight into gross structural changes of a catalyst, this is not sufficient to judge unambiguously the mechanism of catalyst degradation and aggregation.

An alternative approach is to measure the structural changes of NPs after “accelerated aging tests”. Mayrhofer and co-workers recently reviewed reports for performing such an analysis by a technique called identical location/transmission electron microscopy (IL-TEM), which entailed depositing commercial Pt/C NPs on a TEM grid and subsequently using the grid as an electrode.<sup>[231]</sup> After an

electrochemical aging step performed for several hours, the electrode could be inspected with TEM again. Various types of degradation were identified, namely NP detachment, dissolution, and growth. In one case, substantial loss of Pt NPs from the carbon support was observed, which was attributed to detachment rather than dissolution.<sup>[231]</sup> For other catalysts, however, Pt dissolution was observed, particularly for alloyed NPs such as PtCo NPs. An effect of NP dissolution can be the growth of adjacent NPs, through the Ostwald ripening mechanism,<sup>[102,103]</sup> but this has not been observed in IL-TEM measurements, presumably because of the large diffusion distance for Pt ions at the low catalyst loading employed. Although an increase in the apparent NP size was found by IL-TEM, this was mainly attributed to agglomeration. Since these effects were often found to occur simultaneously (even on individual carbon support particles), no generally dominant degradation effect could be determined for the Pt NPs. However, the oxidative shrinking of the carbon catalyst support at elevated temperatures and potentials followed by consequent migration of Pt NPs was found to be a dominant degradation pathway.

These local results could be extrapolated by measuring the loss of electrochemically active Pt surface area, determined through carbon monoxide stripping voltammetry.<sup>[232]</sup> However, since the loss of electrochemical surface area can occur by NP detachment, dissolution, aggregation, or corrosion of the carbon support, electrochemical measurements alone cannot be used to evaluate the exact nature of the catalyst degradation.

Similar degradation measurements were performed by the research group of Muller, where structural information from scanning transmission electron microscopy (STEM) measurements was combined with elemental information from electron energy loss spectroscopy (EELS).<sup>[233,234]</sup> After subjecting commercial PtCo alloy NPs to heat treatment, acid leaching, and 30 000 potential cycles in a PEM fuel-cell setup, it was reported that NPs grew in a synergetic combination of coalescence and Ostwald ripening. By using EELS, the Co and Pt content could be traced inside individual NPs, thereby revealing that the average PtCo core size did not change, while the Pt skin grew significantly as a result of potential cycling, especially at coalesced particles.<sup>[233]</sup>

Muller, Abruña, and co-workers used the same setup for an IL-TEM measurement, in which electron tomography was also applied.<sup>[234]</sup> In this case, the particles were voltammetrically cycled on a carbon-covered Au TEM grid that served as a working electrode in a three-electrode cell (30 000 scans between 0.6 and 1.0 V versus RHE). The cyclic voltammograms (CVs) showed a loss in the electrochemically active surface area of about 20 % (which was also verified using CO stripping) and a concomitant decrease in the ORR activity. By using STEM, the main cause for the surface-area loss could be attributed to NP coalescence, which could be accurately followed using tomography imaging, with no significant change in the size of the PtCo core. Finally, no apparent degradation of the carbon support or significant Ostwald ripening of the catalytic NPs was observed in these controlled experiments,<sup>[234]</sup> in contrast to findings in MEA environments, in which both carbon degradation and NP dissolution have

been observed.<sup>[235,236]</sup> The authors attributed this contrast to the improved potential control of the three-electrode configuration, thereby limiting the relatively mild upper potential limit to 1.0 V, whereas in an MEA the potential can spike up to 1.4 V because of fuel starvation.<sup>[236]</sup>

#### 4. Electrochemistry at Preferentially Shaped Nanoparticles

As highlighted above, the electrochemical performance of metal NPs is typically determined from studies on ensembles of a large number of NPs. However, the inherent dispersion of NP sizes and shapes means that reactivity trends that arise from such studies only reflect the average electrocatalytic behavior of the entire ensemble. Indeed, the overall reactivity of an ensemble may well be dominated by a small fraction of the NPs. These (often poorly reproducible) variations in the dispersion of NP shapes and sizes can make it difficult to compare the findings between different studies. For example, as briefly discussed earlier (Section 1.1), contradicting particle size dependencies have been reported for the ORR as a consequence of difficulties of separating out NP size, shape, coverage, and mass-transport effects. In this section, we will discuss an approach to minimize these variations, while still employing large NP ensembles to perform macroscopic measurements, namely the use of NPs with a well-defined (preferential) shape.

Two seminal papers on the preparation of NPs with a preferential shape through colloidal synthetic methods were reported in 1996 by El-Sayed and co-workers.<sup>[237,238]</sup> By tuning the ratio of the Pt precursor and the capping agent (sodium polyacrylate) during the synthesis, mixtures of NPs were obtained with predominantly tetrahedral, cubic, icosahedral, or cubo-octahedral shapes (Figure 8). This formation of metastable structures (as opposed to the thermodynamically preferred truncated octahedron shape of a metal NP with a face-centered cubic (fcc) lattice) is a result of the anisotropic growth of NPs caused by the preferential adsorption of capping agents and/or other shape-directing agents (such as metal ions) on certain facets during growth, which inhibit the growth of those facets.<sup>[239]</sup> There have been many subsequent reports in which the colloidal synthetic method was adapted to fine-tune the shape of metal NPs of various materials; advances in the colloidal synthesis of shape-controlled particles have been extensively reviewed.<sup>[131,240–245]</sup>

The first electrochemical study of shape-controlled NPs was reported by Feliu and co-workers in 2004.<sup>[69]</sup> The authors employed Pt NPs with preferential {100} surfaces (“cubic” NPs) to study the oxidation of ammonia.<sup>[69]</sup> From studies using macroscopic single-crystal electrodes, this reaction is known to be very sensitive to the structure of the surface, with the reaction taking place almost exclusively at Pt(100) sites, and proceeding faster on larger (100) domains.<sup>[246]</sup> Cubic Pt NPs were found to display a four-times higher specific activity than spherical Pt NPs. This result mirrored that found macroscopically, thus suggesting that single-crystal electrodes could be used to predict structural effects in NPs in this case.

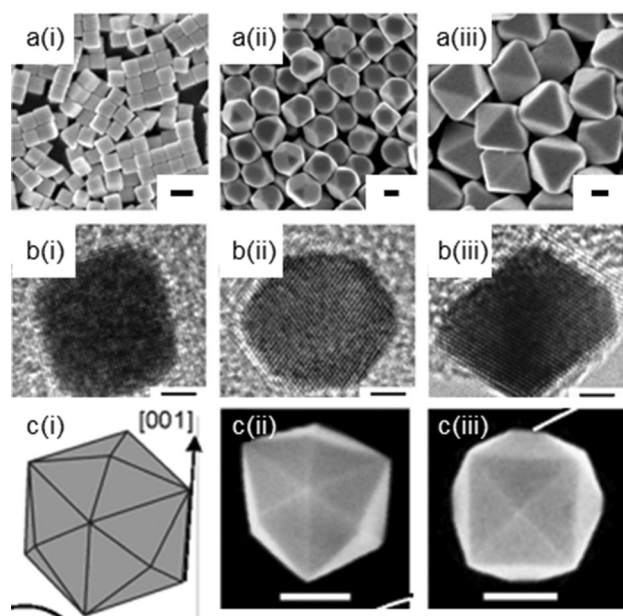


**Figure 8.** Examples of preferentially shaped NPs. a) SEM images of i) cubic (bound by {100} facets), ii) cuboctahedral (bound by {111} and {100} facets), and iii) octahedral (bound by {111} facets) Ag NPs. Scale bar = 100 nm. b) High-resolution TEM images of i) cubic Pt NPs (bound by {100} facets), ii) cuboctahedral Pt NPs (bound by {111} and {100} facets), and iii) octahedral Pt NPs (bound by {111} facets). Scale bar = 2 nm. c) i) Geometric model and ii, iii) SEM images of a tetrahedral-octahedral Pt NP (bound by 24 high-index {hk0} facets, such as {730}). Scale bar = 100 nm. a, b) Adapted from Ref. [244], 2011, Wiley-VCH. c) Adapted from Ref. [94], 2007, American Association for the Advancement of Science.<sup>[94]</sup>

There have been numerous subsequent electrocatalytic studies on “cubic” (predominantly {100} facets, Figure 8a),<sup>[247–256]</sup> “hexagonal” and “octahedral” (predominantly {111} facets, Figure 8b),<sup>[248,255]</sup> and “tetrahedral-octahedral” or “cubo-octahedral” ({111} and {100} facets)<sup>[248,253]</sup> NPs of various (fcc) metals for a variety of reactions.<sup>[245]</sup> Usually, such studies show that the reactivity of preferentially shaped NPs is in qualitative agreement with findings from corresponding single-crystal electrode studies, that is, “cubic” NPs show a (typically, about 3–10 times) higher specific activity than nonpreferentially shaped NPs for reactions that favor (100)-type sites.<sup>[247–256]</sup>

A notable exception to this finding, in which single-crystal reactivity could not be extrapolated to predict the reactivity of preferentially shaped NPs, was reported by O’Mullane, Bhargava, and co-workers.<sup>[255]</sup> The authors compared the reactivity of spherical (rich in {111} facets), cubic (rich in {100} facets), and prismatic (nominally terminated by {111} facets, but rich in defects) Ag NPs for a number of reactions with preferences for different surface sites (oxide formation and stripping, lead underpotential deposition and stripping, hydrazine oxidation, hydrogen peroxide reduction and formaldehyde oxidation), and found that prismatic NPs were the most active for all these reactions. This finding was explained by the high number of defects in the prismatic NPs, thus illustrating that, to study structural effects at the level of an NP, characterizing the number of defects sites is just as

important as tuning the morphology of an NP to expose selected facets.

Although colloidal synthesis has proven successful as a means of generating preferentially shaped NPs terminated by basal plane facets, fundamental studies on macroscopic single crystals have shown that many (electro)catalytic reactions favor low-coordination sites, such as steps, kinks, and defects.<sup>[5,44]</sup> Therefore, shape-controlled NPs enclosed by high-index facets would be desirable to optimize the reactivity of NPs for such reactions. The colloidal synthesis of such NPs is not straightforward due to the high surface energy of high-index facets, which causes them to be eliminated quickly during crystal growth.<sup>[257]</sup> This problem was overcome by Sun, Wang, and co-workers, who have developed an electrochemical method to prepare NPs terminated by high-index facets.<sup>[94,258]</sup> In this method, “large” Pt spheres (ca. 750 nm) were electrodeposited on a glassy carbon electrode. Characterization of these spheres revealed that they consisted of small NPs (of a few nanometers). Subjecting these spheres to a square-wave potential (typically 10 Hz, upper and lower potential: 1.20 V and –0.20 V versus the saturated calomel electrode, respectively) in a solution containing ascorbic acid for 10–60 min caused them to disaggregate into the constituent NPs on the electrode surface. These NPs then underwent dissolution/precipitation cycles to form tetrahedral NPs of 20–220 nm size with 24 {hk0} facets (Figure 8c).<sup>[94,258–263]</sup> NPs of other preferential shapes, such as concave hexoctahedral (enclosed by {hkl} facets),<sup>[264]</sup> trapezohedral ({hkk} facets),<sup>[263,264]</sup> and nanorods (various {hk0} or {hkk} facets)<sup>[264,265]</sup> as well as metals (Pt,<sup>[94,264,266]</sup> Pd,<sup>[261,264,265]</sup> Fe,<sup>[267]</sup> PdPt,<sup>[260]</sup> and PtRh),<sup>[263]</sup> have similarly been produced by adjusting the synthetic conditions.<sup>[257]</sup>

NPs prepared by this method have been employed for a variety of electrocatalytic reactions which are known to be promoted by defects and other low-coordination sites (ethanol oxidation on Pt<sup>[94,262,264]</sup> or Pd,<sup>[261,264,265]</sup> formic acid oxidation<sup>[94]</sup> and nitric oxide reduction on Pt,<sup>[266]</sup> and nitrite reduction on Fe).<sup>[267]</sup> These particles were typically found to have up to four-times higher specific activities than commercially available catalysts, although it should be borne in mind that commercial catalysts are optimized for mass activity (see below) and stability rather than specific activity. A further enhancement in specific activity has been demonstrated by modifying the high-index facets of preferentially shaped NPs with a second metal beneficial for a specific reaction, such as Pd for formic acid oxidation<sup>[260]</sup> or Rh for ethanol oxidation.<sup>[263]</sup> This can be done either by preparing bimetallic particles, such as PtPd<sup>[260]</sup> and PtRh,<sup>[263]</sup> during the synthetic procedure or by surface decoration of preformed (Pt) NPs with adatoms, such as Bi,<sup>[268]</sup> Au,<sup>[269]</sup> or Ru.<sup>[270]</sup>

Although the use of tailored, preferentially shaped NPs (either enclosed by basal planes or by high index facets) is a seemingly straightforward approach to boost the catalytic activity for some reactions, such NPs are quite large (typically > 10 nm for basal plane faceted NPs and 20–150 nm for high-index NPs) compared to commercial catalysts (2–4 nm). Commercial catalysts thus have much better mass activity (current per gram of NP), which is relevant for technological applications, as this ultimately determines the cost of the



catalyst material. Ideally, it would be desirable to decrease the size of the preferentially shaped NPs to the 2–4 nm regime while maintaining the shape to increase the mass activity, but the synthesis of such NPs is challenging.<sup>[259]</sup> Furthermore, smaller NPs of this type are relatively unstable due to lower stabilization from the bulk material, and adsorption and reaction of species during electrocatalysis may cause small NPs to change their shape and lose the enhanced activity.

Sun and co-workers have performed a series of molecular dynamics simulations on Pt NPs with various shapes of ca. 5 nm diameter to address the issue of the stability of preferentially shaped NPs.<sup>[271–273]</sup> Not surprisingly, it was found that truncated octahedrons showed the highest thermal stability, maintaining their shape up to >1000 K, whereas preferentially shaped NPs (both basal-plane NPs and high-index NPs) start to change their overall shape at about 700 K. Although this thermal stability seems sufficient for the employment of preferentially shaped NPs in low-temperature electrocatalytic systems, the issue of electrochemical stability remains to be investigated. In particular, during extended use or repeated start-stop cycles in real applications, the crystal-line surface may not be preserved because of oxidation/reduction cycles.<sup>[274,275]</sup>

## 5. Measurements of Individual Metal Nanoparticles

The ideal model system is a single NP of well-defined shape and size, studied in an electrochemical cell under potentiostatic control. In this section, we will discuss new techniques which have opened up this possibility. Broadly, there are two approaches to study the electroactivity of a single NP (Figure 9).

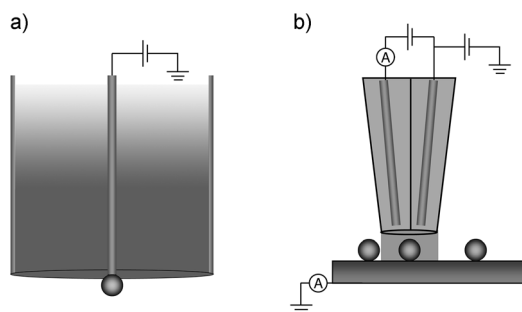


**Figure 9.** Two approaches to study electrochemical reaction at a single NP. a) A single NP is tethered to an NSE (quasireference electrode not shown). b) The response of a single NP within an ensemble is isolated for investigation. In this example, this is achieved with a scanning electrochemical cell microscopy (SECCM) set-up, see Section 5.3.

### 5.1. Techniques and Methods

Significant progress has been made on the use of NSEs, which has allowed the measurement of electrochemical processes at electrodes with dimensions down to nanometer dimensions and often with (sub-)pA currents.<sup>[32,276]</sup> Fabrication methods for such electrodes were initially based on the encapsulation of sharp (etched) wires, akin to scanning

tunneling microscopy (STM) tips, with just the end exposed by sealing in a resist<sup>[277,278]</sup> or by heat-sealing in glass.<sup>[276,277,279,280]</sup> Although very small electrodes can be routinely produced in this fashion, electrodes must be characterized individually before use by a range of techniques to determine the actual electrode surface area. Lithographical techniques allow more freedom in the choice of electrode material. Optical lithography was initially employed for the fabrication of UME arrays<sup>[281,282]</sup> and electron beam lithography has subsequently been employed to prepare individual NSEs.<sup>[283–287]</sup>

Alternatively, instead of decreasing the area of an encapsulated electrode material, the contact area of a macroscopic electrode with the electrolyte can be confined to effectively create an NSE. In scanning electrochemical cell microscopy (SECCM),<sup>[111,288–298]</sup> an electrolyte droplet at the end of a double-barreled theta capillary, which has been drawn to a very sharp tip, contacts a macroscopic electrode surface. Conventional electrochemical measurements can be made between the exposed electrode surface and (quasi-)reference electrodes contained in the barrels. Furthermore, this configuration also allows two-dimensional maps of localized electrode reactivity to be obtained, as discussed in detail in Section 5.3. This technique improves on related microdroplet techniques in terms of the spatial resolution attainable and information content of the experimental data.<sup>[299–303]</sup>

Ideally, to characterize the electrocatalytic activity of metal NPs, one should aim to probe them individually to determine the impact of particle size and shape on catalytic performance directly and unambiguously. However, the direct characterization of the surface of a single NP is extremely challenging. For example, noble metal electrodes are often characterized by measuring the formation and stripping of an oxide monolayer (see Section 2.5) with a charge of approximately  $400 \mu\text{C cm}^{-2}$ .<sup>[192]</sup> For NPs with radii of 10 nm and smaller, this corresponds to about  $10^{-15} \text{ C}$  or less. Measuring such small charges requires very high accuracy current amplifiers with a fast response time, which is a fundamentally difficult combination, although promising results have been reported for state-of-the-art integrated amplifier-electrode systems.<sup>[304,305]</sup> On the other hand, diffusive processes, such as outer-sphere reactions and some electrocatalytic processes (e.g. hydrogen evolution and oxidation, hydrazine oxidation, oxygen reduction) are more readily measurable, as will be shown below. The limiting current at an isolated catalyst NP (with diffusion as the sole mass transport mode) is manifested in a steady-state current [ $I_{ss}$ ; Eq. (1)].<sup>[306]</sup>

$$I_{ss} = nFAk_T C = nFA\chi DC \quad (1)$$

where  $F$  is the Faraday constant,  $n$  is the number of electrons transferred during the reaction,  $C$  is the bulk concentration of the reactant,  $A$  is the surface area of the particle, and  $k_T$  is the mass-transport coefficient, which is the product of a geometry factor ( $\chi$ ) specific to the NP arrangement and the diffusion coefficient of the reactant species ( $D$ ).  $\chi$  is  $\ln(2)/r$  for a sphere on an infinite plane,<sup>[307]</sup>  $1/r$  for a perfect (hemi-)sphere, and  $4/$

$\pi r$  for an inlaid disk, where  $r$  is the radius of the (effective) electrode (NP).<sup>[306]</sup> Taking the four-electron ORR in an oxygen-saturated aqueous solution (at room temperature) as an example ( $C \approx 1 \text{ mM}$ ,  $D = 1.8 \times 10^{-5} \text{ cm}^2 \text{ s}^{-1}$ ), a 5 nm radius spherical particle on a plane gives a steady-state current of about 15 pA, which is well within the capabilities of commercial current amplifiers.

## 5.2. Immobilized Nanoparticle Measurements

One method to measure the electrocatalytic activity of an individual NP is to immobilize it onto a nanoscale support electrode with a low electrochemical background current, thereby ensuring that the NP response can be measured. This approach is exemplified by the work of Chen and Kucernak,<sup>[38,49,308,309]</sup> who electrodeposited a single Pt NP on (the end of) a carbon nanofiber (Figure 10), a support showing

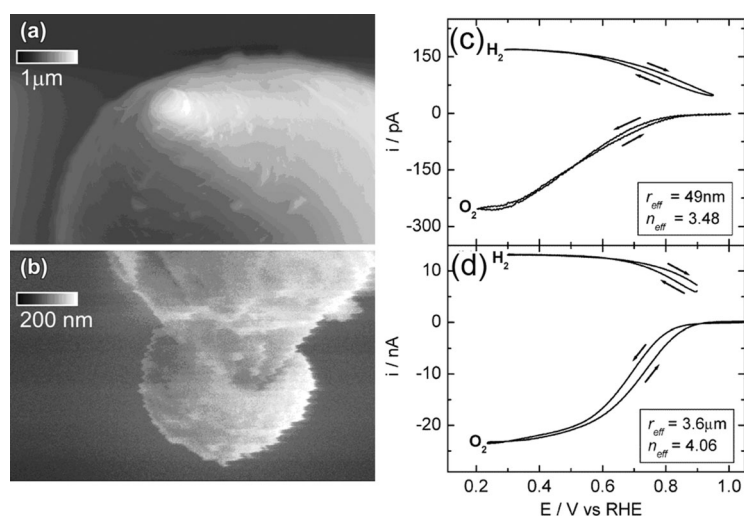


**Figure 10.** a,b) A Pt NP electrodeposited at the apex of a carbon tip. c,d) The kinetics of the ORR and HOR are a function of the radius of the particle as shown for two different radii. Adapted from Ref. [38] (2003, American Chemical Society) and Ref. [309] (2004, American Chemical Society).

negligible Faradaic activity over a wide range of potentials.<sup>[308]</sup> The nanofiber was first sealed in a layer of electrophoretic paint with only the apex left uncoated to minimize the conductive area. Subsequently, Pt was electrodeposited using potential pulses of well-defined duration, with the pulse length correlating to the final particle radius.<sup>[38]</sup> In this way, the influence of the NP radius on the kinetics of the ORR and HOR was investigated.<sup>[49,309]</sup> For the ORR (in 0.1M  $\text{H}_2\text{SO}_4$ ), an effective number of electrons  $n_{\text{eff}}$  of 3.5 was found in the diffusion-limited regime for NPs smaller than 100 nm. This number was inferred from the diffusion-limited current using Equation (1), for which  $\chi$  was determined using the HOR ( $n=2$ ) on the NP electrode, and  $D$  was obtained from UME measurements.

The effective number of electrons transferred per  $\text{O}_2$  molecule depends on the relative yields of hydrogen peroxide (2 electrons per  $\text{O}_2$  molecule) and water (4 electrons per  $\text{O}_2$

molecule). A transfer of only 3.5 electrons per oxygen molecule implies that 25% of the oxygen is converted into hydrogen peroxide without reacting further to water (see Figure 2, Section 1.1). For particles smaller than 100 nm, the mass transport ( $k_T \geq 2 \text{ cm s}^{-1}$ ) is so fast that some of the  $\text{H}_2\text{O}_2$  produced escapes the electrode vicinity and is transported into the bulk electrolyte. These findings are consistent with the proposed mechanism on the role of mass transport in NP ensembles outlined in Section 3, at least qualitatively. It should be noted that these measurements were conducted without detection of hydrogen peroxide, which would have underpinned the mechanistic interpretation of the data.

The extremely fast mass transport to and from individual NPs allows the study of reaction mechanisms in potential regimes where the current is normally dominated by diffusion limitation (e.g. in rotating disk electrode measurements). Thus, no clear mass-transport-limited current was observed for particles smaller than 50 nm ( $k_T \geq 4 \text{ cm s}^{-1}$ ). It was reasoned that significant kinetic limitations under these high mass-transport conditions pushed the ORR into the potential domain where hydrogen adsorbs on the Pt surface ( $\text{H}_{\text{UPD}}$ ).

In the HOR, the high mass-transport conditions of the experiment allowed the observation of an extra current plateau in the  $\text{H}_{\text{UPD}}$ . By fitting the CVs by a kinetic model, the Tafel–Volmer mechanism was found to be the dominant mechanism rather than the Heyrovsky–Volmer mechanism (see Section 1.1).<sup>[49]</sup>

Individually electrodeposited particles were also used in a study by Tel-Vered and Bard,<sup>[310]</sup> where a carbon fiber, biased at the Pt electrodeposition potential, was covered with a film of electrophoretic paint containing pinholes. As the fiber was gradually immersed into a solution containing  $\text{Pt}^{\text{II}}$  ions, a cascade of reduction transients was measured as a function of the tip immersion depth, thus indicating Pt deposition at the pinholes. A subsequent slow immersion into a fresh electrolyte containing  $\text{Fe}^{3+}$  ions (enhanced reduction kinetics on Pt with respect to C) showed discrete increases in the reduction current as the freshly generated Pt NPs gradually came into contact with the solution, so that the contributions of the different particles were separated in time and space.

Poor control over NP shape is a major disadvantage (Section 2.1) of using electrodeposition to immobilize a particle on an electrode, and particle stability on the support has been reported to be problematic.<sup>[310]</sup> To circumvent these problems, single colloidal NPs with fine-tuned shape and size can be attached from a dilute colloidal solution to an NSE with a radius equal to or smaller than the NP size.<sup>[154,168,311]</sup> However, it is not trivial to produce, handle, and characterize NSEs with radii below 10 nm,<sup>[312–315]</sup> and there is a restriction on the choice of electrode materials.<sup>[316]</sup>

Zhang and co-workers immobilized a single Au NP on an oxidized Pt NSE through a silane linker terminated with an amino group. An individual NP was found to adhere to the modified electrode (in TEM analysis) when it was immersed

in a solution containing NPs.<sup>[154]</sup> Similarly, Sun and co-workers reported the attachment of a single Pt NP on an Au NSE through an alkanethiol linker.<sup>[168,313]</sup> In another experiment, the surface of a Pt NSE was not modified, but cycled voltammetrically in a solution containing Au colloid. When a reduction current was observed in the CV, this was interpreted as the arrival of a single Au NP.<sup>[311]</sup> Electrochemical analysis of these individual probes included the deposition of Cu monolayers<sup>[154]</sup> and the measurement of Au-blank CVs in sulfuric acid.<sup>[154,311]</sup> Both of these methods can be employed to determine the electrochemically active surface area of an electrode,<sup>[192]</sup> but as mentioned earlier, such surface electrode measurements are challenging, and in these particular studies the surface area was significantly overestimated compared to ex situ electron microscopy measurements. The authors tentatively rationalized this by suggesting that the bulk Au atoms were also oxidized in addition to the surface atoms, thus leading to Au reduction charges higher than expected.<sup>[311]</sup> Unexpectedly, ORR measurements revealed a lower overpotential for Au NPs compared to the bare Pt disk UME, but a much smaller diffusion-limited current, which suggests that the Au NP was not participating fully in the reaction.<sup>[154]</sup> Regardless of these inconsistencies, these experiments indicate the possibility of immobilizing single-catalyst NPs and studying their reactivity, and we anticipate much further development in this field.

Rather than immobilizing the NP on a very small electrode, one might choose to deposit particles at a known location on a macroscopic electrode by using the high spatial resolution afforded by scanning probe techniques, such as scanning tunneling microscopy (STM; Figure 11). Once the

NP is on the macroscopic electrode and located by the STM tip, it is biased to promote an electrochemical process of interest, and the probe tip (moved back by ca. 10 nm) then serves as a collector electrode to detect any generated products in an SECM-type configuration. In this way, the HER kinetics at a single Pd particle were studied by applying different potential pulses to the substrate and measuring the collector current.<sup>[54]</sup> The reaction rates were found to decrease with increasing NP height (total amount of Pd layers). In fact, NPs consisting of less than five Pd layers were found to be orders of magnitude more reactive than those with more layers. This effect was modeled using density functional theory calculations, and it was interpreted as arising from the strain induced on the Pd NP because of the lattice mismatch with the underlying Au(111) substrate. The strain increases the average Pd-Pd distance, on which the HER reactivity is primarily dependent.<sup>[317]</sup> Although this method presents an elegant way to study the effect of size on electrocatalysis at a single NP, the interpretation of the experimental results is not straightforward and has led to considerable discussion.<sup>[318]</sup> Nonetheless, this type of measurement demonstrates the insights offered by SECM-type measurements using ultra-small probes.

### 5.3. Nanoparticle Landings

It is not necessary to preimmobilize NPs on an electrode as in the approach described in Section 5.1; their arrival at electrodes from a (dilute) colloidal solution may also be detected electrochemically. When an electrocatalytically inert

UME is immersed into a solution containing both a reactant and a catalyst NP, on which that reactant can be turned over, a current signal is measured whenever an NP is polarized by colliding with the UME. This approach can be traced to the studies of Heyrovsky et al., who showed that the reduction of polydisperse ceramic semiconductor NP colloids contributed to the cyclic voltammetry of an Hg drop electrode by a summation of cathodic steps that had an onset potential dependent on the particle size.<sup>[319–322]</sup> In a later study on the interaction between metallic NP colloids and an Hg electrode it was found that

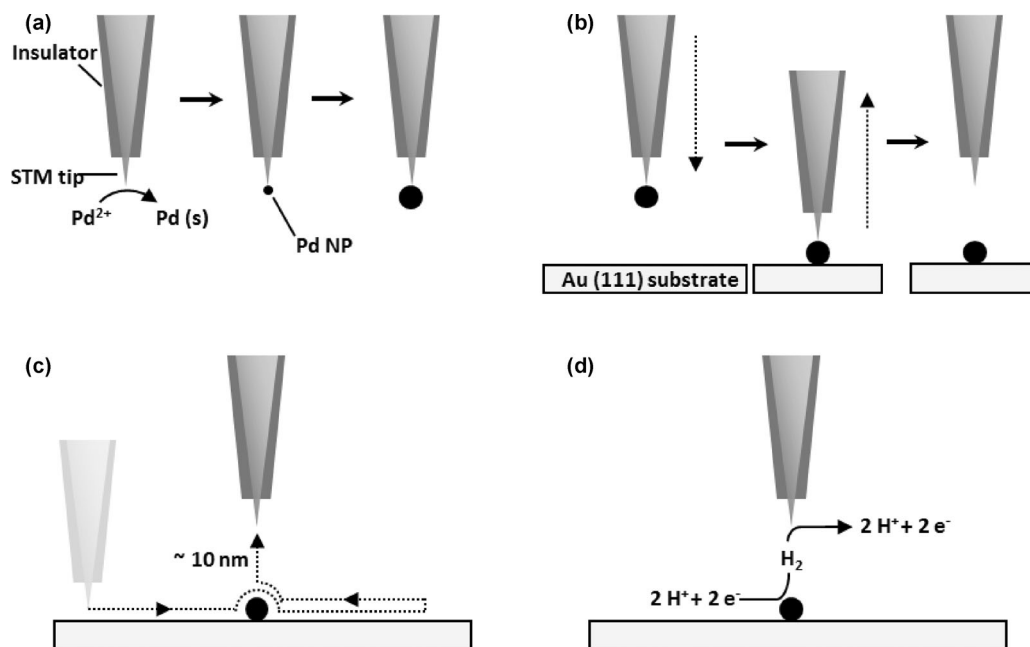


**Figure 11.** Schematic representation of the single NP experiment by Stimming and co-workers.<sup>[54]</sup> A Pd NP is formed through electrodeposition at the tip of an STM probe (a), and then deposited onto an Au surface (b). The surface-immobilized NP is imaged with the tip (c) and the tip is then moved back 10 nm and used in the “collector-mode” (i.e. as an SECM tip) to detect  $\text{H}_2$  produced by electrocatalysis at the NP (d). Adapted from Ref. [219]. 2012, Cambridge University Press.



the cathodic waves measured consisted of discrete contributions from the reduction of the oxidized NPs arriving at the electrode.<sup>[323]</sup> It has also been demonstrated that the faradaic current at a UME performing a redox reaction decreased in discrete steps upon the addition of insulator microparticles. Optical microscopy indicated that the blocking of the electrode by these particles was the cause for the diminished current.<sup>[324,325]</sup>

The first detection of NPs through electrocatalytic amplification (Figure 12) was demonstrated by the Bard research group by using a carbon UME with Pt NPs in solution that was held at a potential at which hydrogen evolution would occur on Pt but not on carbon. Current spikes were detected with a frequency that could be roughly correlated with the expected diffusional flux of NPs toward the electrode surface (see below).<sup>[307]</sup> This type of experiment has since been reproduced by several research groups for a number of combinations of the electrode material, the NP material, and the reactant molecule, as well as variations in the experimental set-up and coupling with other techniques (see Table 1). Broadly speaking, two distinct types of reactivity have been observed: a cumulative cascade of current steps (“a staircase”) and a series of transiently decaying current jumps (“spikes”). A current staircase is expected for the landing of NPs on an electrode that catalyzes a reaction continuously. Current spikes are observed when NPs continuously arrive at a surface, but their reactivity is finite.

The heights of the electrocatalytic current steps measured when NPs land on an electrode can, through Equation (1), provide an insight into the particle size. This is illustrated well by several studies of the oxidation of hydrazine at Pt NPs landing on Au UMEs,<sup>[294,326–329]</sup> where the landing frequency and current step height distributions were in reasonable agreement with the concentration and size distribution of the NPs determined by other methods, such as TEM.<sup>[326]</sup> However, it should be noted that the size of NPs can only be determined accurately from diffusion-limited reactions if the diffusion coefficient of the reactant molecule is known or can be determined with a high degree of certainty. This may appear to be a trivial and obvious point, but is particularly troublesome for hydrazine, a popular reactant for this type of experiment, for which the reported diffusion coefficients show a significant spread, ranging from about  $10^{-8}$  to  $10^{-3} \text{ cm}^2 \text{ s}^{-1}$ , with typical values between  $0.6$  and  $2.0 \times 10^{-5} \text{ cm}^2 \text{ s}^{-1}$ .<sup>[55,56,330–333]</sup> This has a corresponding impact on the use of amperometry to determine NP size, since the limiting current depends linearly on the diffusion coefficient [Eq. (1)].

To confirm that Pt NPs catalyze the hydrazine oxidation, Bard and co-workers studied the effect of treating the particles or the UME with self-assembled monolayers (SAMs).<sup>[327]</sup> After treating a UME with an alkanethiol with a chain length up to 12 methylene units, landings of as-prepared (citrate-capped) Pt NPs could still be detected, but the magnitude of the current step per landing decreased as the chain length increased. The authors suggested this to be due to the suppression of electron tunneling from the NP through the SAM to the UME,<sup>[327]</sup> although this would appear to contradict the Chazalviel–Allongue model (see Sec-

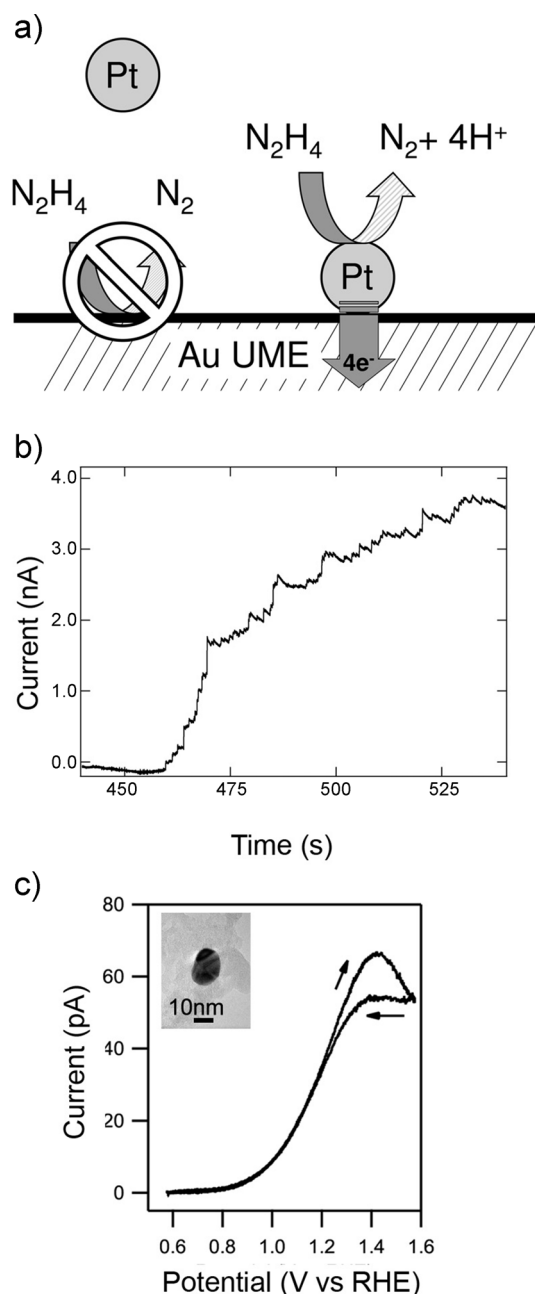


**Figure 12.** a) An inert UME is in a solution containing an electrocatalytic reactant and catalyst NPs. As the NPs impact the surface they convert the reactant and a current is measured. b) If the NPs stick to the surface, the current contribution is continuous, thereby resulting in a staircase-type current–time plot, such as at an Au UME in the presence of Pt NPs in a hydrazine-containing solution. c) Cyclic voltammogram ( $200 \text{ mVs}^{-1}$ ) for the oxidation of 2 mM hydrazine at a single Au NP (shown in inset) on a TEM grid electrode. Adapted from Ref. [328] (2013, American Chemical Society) and Ref. [294] (2012, American Chemical Society).

tion 2.3).<sup>[183]</sup> Conversely, if the NPs were capped with an alkanethiol SAM, the ability to detect their landing was significantly reduced when the length of the carbon chain was increased; a much lower landing frequency was detected even for the shortest chain length of three carbon atoms. Capping the NPs with other stabilizing molecules typically used in NP

**Table 1:** Comparison of landing frequencies of NPs measured in different reports.<sup>[a]</sup>

Landing frequency [10 <sup>4</sup> s <sup>-1</sup> μm <sup>-1</sup> cm <sup>-2</sup> ]	Reaction	Response type	NP material/size	UME material/radius	Reference
8.0	HER	spike	Pt/4 nm	C/4 μm	[307]
2.4–4.0	N <sub>2</sub> H <sub>4</sub> oxidation	staircase	Pt/4 nm	Au/5 μm	[326]
1.3–0.71	NaBH <sub>4</sub> oxidation	spike	Au/14 nm	PtO/5 μm	[336]
8.9	OER	spike	IrO <sub>x</sub> /28 nm	Pt/5 μm	[337]
0.0071	N <sub>2</sub> H <sub>4</sub> oxidation	staircase	Pt/4 nm	Au*/2000 μm <sup>2</sup>	[328]
4.0	various redox processes	staircase	Au/20 nm	C†/0.5 μm	[294]
3.9	Ag NP oxidation	spike	Ag/20–50 nm	C/11 μm	[339]
2.4	Th UPD	spike	Ag/45 nm	C/11 μm	[341]
3.2	Cd deposition	spike	Ag/45 nm	C/11 μm	[342]
4.1	Ag NP oxidation	spike	Ag/14, 29, 45 nm	C/11 μm	[343]
5.2	H <sub>2</sub> O <sub>2</sub> reduction.	spike	Ag/14 nm	C/5 μm	[344]
2.6	nitrothiophenol oxidation	spike	Ag/45	C/11 μm	[345]
0.33–0.49	N <sub>2</sub> H <sub>4</sub> oxidation	spike	Pt/4, 12, 22 nm	Hg@Pt/12.5 μm	[329]
0.25	N <sub>2</sub> H <sub>4</sub> oxidation	<sup>[b]</sup>	Pt/16 nm	Au/5 μm	[346]

[a] Measurements were made at disk-shaped UMEs, except where a rectangular, lithographical electrode was used (\*) and measurements performed in a (SECCM) droplet cell setup (†). [b] Detection by measuring change in the open-circuit potential.

synthesis, such as polyvinylpyridine (PVP) and cetyltrimethylammonium bromide (CTAB) resulted in a similar loss of ability to detect collisions. These findings were rationalized as follows: hydrazine oxidation requires certain catalytic surface sites on the NP, which are blocked by strong capping agents, whereas ET from the NP to the UME is governed by electron tunneling (and is thus relatively insensitive to the nature of the capping agent).<sup>[327]</sup> Aside from proving the proposed mechanism of detection for NP landing, this method could also be used to evaluate charge transfer between an NP and an electrode through SAMs comprised of organic molecules.

The inability to detect NPs after changing the NP capping is one reason why the majority of successful NP landing experiments makes use of citrate-capped NPs. The interaction between citrate and the NP metal surface is such that the surface reactivity is not hindered significantly, while electrostatic repulsion between NPs in solution limits aggregation. The adsorption strength of citrate on Au surfaces is comparable to that of anions such as sulfate,<sup>[334,335]</sup> which is known to diminish, but not block, catalytic reactivity,<sup>[44]</sup> while organic molecules such as PVP and CTAB have a stronger surface interaction and tend to inhibit catalytic activity more significantly.<sup>[184]</sup>

Rather than using conventional glass-sealed UMEs, Kleijn et al. employed lithography to fabricate Au UMEs as the support electrode for NP landings.<sup>[328]</sup> They found that the landing frequency for Pt NPs (using hydrazine or hydrogen as the reactant) was much lower than expected and that the distribution of current-step magnitudes from a series of landings showed significant tailing at higher current values.<sup>[328]</sup> Both the lower landing frequency and the observation of larger currents indicated a reduced effective NP concentration, which was attributed to the aggregation of NPs in solution. Aggregated NPs were observed on the support electrode by SEM after a landing experiment. However, when NPs landed in the absence of hydrazine or hydrogen, no aggregates were detected on the UME, thus demonstrating that NPs in solution can aggregate by interaction with the reactants added for NP detection. It was proposed that the

weakly bound citrate molecules were displaced by the hydrazine or hydrogen and that the diminished electrostatic repulsion resulted in aggregated NPs.

An alternative platform to prepare an electrode for NP landing experiments is by using SECCM, as recently introduced by Unwin and co-workers.<sup>[294]</sup> An SECCM probe, containing an electrolyte solution with Au NP colloids, was moved slowly towards the working electrode until the meniscus at the end of the pipette made contact with the conductive substrate, thereby forming a nanoscopic electrochemical cell to perform NP landing experiments. Compared to the landing experiment describe above, in which preformed UMEs were used, this approach offers several key advantages. First, a wide range of materials can be used for the support electrode, as no traditional UME manufacture is required. Second, the cell can be made and disconnected at will on a millisecond timescale at specified locations. Finally, ultrasmall electrode areas can readily be achieved by employing pipettes with smaller diameters, thus offering a significant decrease in background current.

The high sensitivity of this approach was demonstrated by measuring Au NP landing experiments on highly oriented pyrolytic graphite, a carbon support with very low background currents with which it is unfeasible to prepare a UME or NSE by conventional methods. The landing of Au NPs was detected over various potentials for the ORR and HER processes, including potentials at which the magnitude of the individual current steps was less than 1 pA. The versatility in the choice of substrate was further emphasized by landing Au NPs onto the carbon foil of a TEM grid, which was connected as a working electrode, using the oxidation of hydrazine as a probe reaction. After the first current step (indicating the arrival of a single NP at the TEM grid), the tip was retracted and the grid was characterized by TEM, thus allowing a correlation to be made between the current magnitude of the landing step and the NP size. An estimation of the NP sizes from the current responses, by using Equation (1), provided values that were in good agreement with the actual NP sizes.<sup>[307]</sup> Additionally, a cyclic voltammogram of hydra-

zine oxidation on a single gold nanoparticle could be measured (see Figure 12c). This approach has considerable promise for structure–reactivity measurements at the single NP level.

Bard and co-workers have diversified combinations of NP metals and electrocatalytic reactants that can be studied by NP landing. Thus, Au NPs were detected through the oxidation of borohydride, which can be suppressed on Pt UMEs that have been preoxidized. These collision measurements showed spiked responses, thus suggesting that the NPs either desorbed from the electrode surface or stayed in place, but became deactivated.<sup>[336]</sup> Similar results were found for the detection of iridium oxide (IrO<sub>x</sub>) NPs using the OER. Since IrO<sub>x</sub> is more active than Pt for the OER, current spikes could be observed at a potential just below the onset of the OER current on Pt UMEs.<sup>[337]</sup> To gain additional insight into the current decay transient observed for IrO<sub>x</sub> NPs, the landing detection was performed in an SECM configuration where a macroscopic surface (2 mm diameter Pt disk) and a Pt SECM tip (5 μm radius) were held in proximity (i.e. 50 μm separation) and biased at the same potential (0.8 V versus Ag/AgCl).<sup>[338]</sup> NP landings were monitored at the SECM tip, while the macroscopic disk acted as an NP sink (shielding experiment). The landing frequency of IrO<sub>x</sub> NPs was seen to decrease as a function of time, as a result of NP adsorption at the macroscopic electrode. It was thus deduced that the current–time transient for the OER at IrO<sub>x</sub> NPs was due to irreversible sticking and subsequent deactivation rather than to an intermittent contact between the NP and the collector UME.

The Compton research group<sup>[339]</sup> has adopted the NP landing method to measure the size distribution and concentration of NPs in solution, through a method coined “anodic particle coulometry” (APC).<sup>[340]</sup> When an NP contacts a glassy carbon UME that is held at a potential to promote electrodisolution of the metallic NP to its constituent ions, an anodic current–time transient is measured. By measuring the charge transferred in the transient, the amount of atoms per NP can be determined, and the original particle size distribution can be derived if the average particle shape is known.

The formation by electrodeposition of a metal shell on an NP upon impact has also been reported: current peaks were measured at potentials below the Ag oxidation potential for impacting Ag NPs in the presence of ionic thallium<sup>[341]</sup> or cadmium.<sup>[342]</sup> The integrated charge passed during each spike could be related to the number of monolayers of metal deposited on the NP. Depending on the applied potential and the depositing metal, both the underpotential deposition (UPD) and the bulk deposition of metals could be achieved. The oxidation of adsorbed molecular monolayers from metal NPs was also shown in another study to be measurable.<sup>[345,347]</sup>

The landing of Pt NPs at an Hg-modified Pt UME has also been reported by Stevenson and co-workers.<sup>[329]</sup> Since Hg is a very inert electrode material for electrocatalysis, it is an interesting candidate to use for the electrocatalytic detection of NP landings, as illustrated earlier in the pioneering studies of Heyrovsky et al. on NP detection.<sup>[319–322]</sup> First, a thin film of Hg was formed on the Pt UME by electrodeposition. The Pt

NP landings were then measured by the oxidation of hydrazine, which appeared as spikes rather than a staircase response. It was argued that the Hg thin film passivating the Pt UME amalgamates with the Pt NPs, thereby deactivating them.

### Quantitative Analysis of Nanoparticle Landing Measurements

Attempts have been made to correlate the NP landing frequency to the diffusion-based mass transport of particles towards the collector electrode, which is assumed to occur when an NP concentration gradient builds up near the electrode, which acts as a sink for NPs.<sup>[348–351]</sup> The landing frequency is then expected to scale with the UME radius, determined from the diffusion-limited flux function for an in-laid microdisk geometry [Eq. (5); analogous to Eq. (1)]:

$$f_{\text{NP}} = 4 N_A D_{\text{NP}} C_{\text{NP}} r_{\text{UME}} \quad (5)$$

where  $f_{\text{NP}}$  is the landing frequency,  $N_A$  is the Avogadro constant ( $N_A = 6.022 \times 10^{23} \text{ mol}^{-1}$ ),  $D_{\text{NP}}$  is the diffusion coefficient,  $C_{\text{NP}}$  is the NP bulk concentration, and  $r_{\text{UME}}$  is the disk radius of the UME. The NP diffusion coefficient can be estimated from the Stokes–Einstein Equation [Eq. (6)]:

$$D_{\text{NP}} = \frac{k_B T}{6 \pi \eta r_{\text{NP}}} \quad (6)$$

where  $\eta$  is the dynamic viscosity of the solution ( $\eta \approx 8.90 \times 10^{-4} \text{ Pa s}$  for dilute aqueous solutions),  $r_{\text{NP}}$  is the NP radius,  $k_B$  is the Boltzmann constant ( $k_B = 1.381 \times 10^{-23} \text{ J K}^{-1}$ ), and  $T$  is the temperature. However, landing frequencies predicted from the simple diffusion model of Equation (5) consistently overestimate the landing frequency compared to the experimental data in Table 1.

Experimentally, the landing frequency has been shown to correlate with the radius of the electrode,<sup>[348]</sup> the concentration of the NPs,<sup>[326,329,339,348]</sup> and the viscosity of the solution.<sup>[348]</sup> However, the NP size should also influence the landing frequency, as the diffusion coefficient depends reciprocally on the NP radius ( $r_{\text{NP}}$ ) through Equation (6). Therefore, as the NP size is increased, the NP diffusion rate and consequentially the NP-UME collision frequency should decrease. An order of magnitude difference in the diffusion coefficient is expected for the NPs reported in the literature with radii in the range of 2 to 25 nm (as summarized in Table 1). However, such a correlation is not evident, even though many different NP sizes have been studied to determine the influence of the NP radius on the magnitude of the current response.<sup>[326,329,339]</sup>

The apparent overestimation of landing frequency when using Equation (5) suggests that this equation does not model real NP landings particularly well, and that a more detailed model should be formulated. Attempts at modifying the original model have been made, for example, by the introduction of a factor that takes into account that not every collision results in NP sticking, and not every sticking NP might yield a measureable response.<sup>[348]</sup> Another possible explanation for the diminished collision frequency could be



the result of NP collisions on the insulating sheath surrounding the inlaid metal electrode. The area of the sheath is typically several orders of magnitude larger than that of the collector electrode, and if the sticking probability of NPs onto the sheath was finite, it could act as an NP sink and effectively shield the collector electrode.

Another issue in the quantitative description of NP collisions is that the shape of the current response measured does not always match the expected behavior. For example, in the case of the HER on Ag NPs<sup>[339]</sup> or Pt NPs<sup>[307]</sup> on GC UMEs, current spikes are detected rather than the staircase expected for NPs at which the electrocatalytic reaction is continuous. On other carbon substrates (HOPG and TEM grid C foil),<sup>[294]</sup> a staircase-type increase in the current has been reported for the hydrazine oxidation and ORR, thus indicating cumulative sticking of NPs on the electrode surface. Moreover, current spikes are detected instead of a staircase response for the oxidation of  $\text{NaBH}_4$  on Au NPs<sup>[336]</sup> and oxygen evolution on  $\text{IrO}_x$  NPs<sup>[337]</sup> at passivated Pt electrodes. Also, the detection of Pt and Au NPs on boron-doped diamond UMEs through the hydrazine oxidation reaction showed a staircase response for Au NPs and current spikes for Pt NPs.<sup>[352]</sup>

Interestingly, landing frequencies obtained with the different characteristic current responses (i.e. spike or the staircase characteristic) are very similar, even though it has been suggested that the spike response corresponds to a nonsticking interaction with the electrode. It was reasoned by Bard and co-workers that the interval in which a nonsticking NP is in proximity to the electrode to experience multiple collisions is too short to be resolved with conventional electrochemical techniques.<sup>[348]</sup> Therefore, the UME-NP interactions are “bunched” into a common current response. The frequency of the current response is then equivalent to the diffusion of the NPs towards the electrode, and the landing frequency is that of sticking particles. Thus, the landing frequency cannot be used to distinguish between different interactions of the NP and the UME.

It is difficult to differentiate between sticking followed by deactivation and a transient, “bouncing” interaction solely on the basis of electrochemical NP landing detection since the transient electrochemical signal and the landing frequency alone do not contain enough information to make this distinction. The staircase responses measured in electrocatalytic NP sticking experiments also show a decay on a long (i.e. seconds) timescale.<sup>[326,328]</sup> The charging time of the double layer, or the electrical time constant of the measurement system is much smaller than this, and does not explain the current decay. Physical effects, such as the contamination of the catalytic surface by trace amounts of poisonous species in the electrolyte, could cause the transient effect by deactivating the NP. The research groups of Koper and Unwin used electron microscopy to show that, after landing had been detected through a staircase current, NPs remained on the electrode after the detection measurement.<sup>[294,328]</sup> The current spikes

observed by Kwon and Bard during the landing of  $\text{IrO}_x$  NPs were shown by using SECM to be due to NP deactivation, rather than desorption,<sup>[338]</sup> although ex situ electron microscopy would provide a more definitive conclusion for such studies.

### 5.3. Measurements at the Single Nanoparticle Level within Nanoparticle Ensembles

Recently, there has been a renewed impetus to study NP ensembles at a single NP level through the development of novel techniques. One such technique is SECCM, discussed briefly above and shown in more detail in Figure 13a.

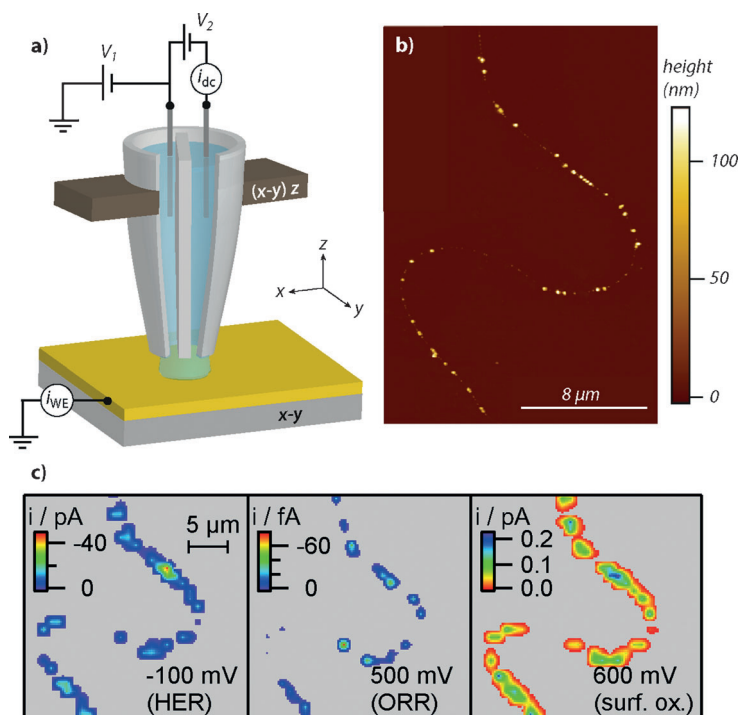


**Figure 13.** a) Schematic representation of a scanning electrochemical cell microscopy (SECCM) set-up. Adapted from Ref. [298]. b) AFM image of Pt NPs deposited on a single carbon nanotube. c) SECCM images of the same area as in (b) at  $-100$  mV (HER),  $500$  mV (ORR), and  $600$  mV (surface oxidation) versus  $\text{Pd-H}_2$ . Adapted from Ref. [111]. 2011, American Chemical Society.

SECCM employs a dual-barrel (theta) pipette as a probe, pulled to a sharp point with a laser puller to the desired dimensions (ca.  $100$  nm to  $50$   $\mu\text{m}$ ). Ultimately, the dimensions of the pipette determine the spatial resolution of SECCM. After rendering the outer wall of the pipette hydrophobic, both barrels are filled with an electrolyte solution of interest, and a quasireference counterelectrode is inserted into each barrel. A small potential bias is applied between the two quasireference counterelectrodes (QRCEs) to induce an ionic conductance current across the electrolyte meniscus at the end of the tip. The potentials of the QRCEs can be floated with respect to the ground potential, while maintaining the

potential bias between them, to set the effective potential at the substrate, which is held at the ground potential.

To obtain two-dimensional maps of substrate reactivity the electrolyte meniscus at the end of the pipette is brought into contact with the substrate. This is aided by a small oscillation (typically 10–30 nm) applied to the pipette in the direction perpendicular to the substrate, which causes a periodic deformation of the meniscus and gives rise to an alternating current (ac) component to the ionic conductance current. The magnitude of the ac is strongly sensitive to the distance between the end of the pipette and the substrate, and can be used as a feedback parameter to maintain a constant separation while scanning across the surface, thereby producing two-dimensional maps of surface activity and surface topography simultaneously.

By employing pipettes smaller than the average interparticle distance, Lai et al. studied electrocatalytic Pt NPs within an ensemble directly with SECCM (Figure 13).<sup>[111]</sup> The Pt NPs were prepared by electrodeposition on a single, isolated carbon nanotube supported on a silicon/silicon oxide wafer. The carbon nanotube served not only as a template for electrodeposition, but also as a nanoscopic wire to electrically connect the NPs (Figure 13b). Typical maps of surface activity obtained with SECCM are shown in Figure 13c. Comparing the activity maps with the AFM image shows there is an excellent correspondence between the electrocatalytically active regions and the location of the individual NPs. SECCM maps were obtained at various potentials, corresponding to surface oxidation processes as well as the ORR and the HER. Measuring the potential-dependent electrocatalytic response of individual NPs and correlating it with the size and structure obtained by AFM and SEM resulted in several notable findings. First, the reactivity of individual NPs was highly non-uniform, with subtle changes in NP size and shape leading to significant changes in activity. Furthermore, different NPs displayed different current–potential profiles, even though the average current over the total ensemble yielded an “expected” potential-dependent current profile. In some cases, NPs that were active for the ORR showed no activity towards the HER. Finally, the study also demonstrated the very high sensitivity of this new technique, being able to measure currents of about 10 fA over a 40 ms measuring time, which corresponds to the reduction of about 600 O<sub>2</sub> molecules (assuming a four-electron transfer process).

A recent report demonstrates the ability of a combined AFM-SECM approach to measure electrochemistry at individual NPs.<sup>[353]</sup> In their study, Demaille and co-workers dispersed Au NPs on a substrate covered with an alkanethiol SAM, and modified the NPs with a redox-labeled ferrocene/polyethylene glycol capping agent (Fc-PEG). A conductive AFM tip with a radius of about 100 nm was used to turn over the redox strands shrouding the NPs and measure the corresponding current response. A variance in NP activity was detected, as only about 80 % of the NPs measured by AFM in the topography mode generated a measurable SECM current. Demaille and co-workers attributed this to the unsuccessful grafting of the Fc-PEG at possibly contaminated NPs, as in a separate conductive AFM experiment they showed that approximately 90 % of the NPs were in fact

electronically coupled to the substrate electrode. It should be noted that the SECM currents were rather small compared to the background signal and significant signal processing and digital filtering were needed to extract the SECM currents (ca. 300 fA).

Another recent technique to study individual NPs within an array employs an optical method based on surface plasmon resonance (SPR).<sup>[354]</sup> SPR is rather sensitive to variations in the refractive index near a metal surface,<sup>[355]</sup> and refractive indexes change when reactants are converted at an electrode surface.<sup>[356]</sup> This method was applied to detect hydrogen evolution at an array of NPs. A CV was recorded on the entire ensemble while following localized changes in the SPR, which could be related to single NPs. Apparent CVs for individual NPs could be reconstructed using the potential-dependent SPR changes of the NPs.<sup>[354]</sup> For Pt NPs with a diameter of 80 nm, a wide variability from one NP to the next in the HER current was found at a potential of –0.2 V versus RHE, which is similar to the changes in activity observed in the studies by Lai et al. highlighted above.<sup>[111]</sup>

Electrochemical strain microscopy is also emerging as an insightful technique for probing electrocatalytic activity on the nanoscale in certain environments. This technique can be used to detect catalytic effects of individual NPs in a model solid-oxide fuel-cell environment.<sup>[357]</sup> In this study, a platinized tip of an AFM was placed in contact with a surface that conducted oxygen ions (yttrium-stabilized zirconia; YSZ) in ambient air. A potential bias was then applied that resulted in the ORR/OER reaction at the tip, thereby leading to a diffusion of oxygen vacancies in the YSZ lattice towards the surface. The movement of vacancies resulted in strain that could be detected by the probe as surface deformations on the pm level. When the tip was on or near a catalyst NP, the applied bias also affected the NP, resulting in enhanced ORR/OER. In this way, and using the ORR/OER system, an electrochemical map was made of Pt nanoislands evaporated onto a YSZ support, on which the Pt areas had the highest ORR/OER activity. So far, as a result of the ultralocal nature of the probe (i.e. the tip is much smaller than the nanoparticles), no quantitative information regarding the shape and size dependence of the catalytic activity could be obtained, although these studies further highlight how local probes have considerable prospects for unraveling the activity of complex NP electrocatalysts.

## 6. Conclusions and Outlook

In this Review, we have highlighted and discussed recent reports on the electrochemistry of NPs, with particular attention given to electrocatalytic processes which are among the most widely studied. Although a wide range of NP configurations has been considered, from extensive ensembles to individual NPs, the focus has been on studies which provide enhanced (quantitative) information on NP activity through investigations characterized by well-defined mass transport and/or making use of NPs of highly defined architecture, or where structure can be measured and related to activity at the single NP level.

Much progress has been made in controlling the shape and size of NPs, particularly during the colloidal synthesis of NPs. Many different shapes can be made reliably and these shape-tailored NPs typically show electrocatalytic responses reminiscent of their dominant exposed surface facets in single-crystal measurements. However, most shape-controlled NPs are still very large compared to commercial catalyst NPs and, therefore, have suboptimal mass activity. Additionally, the morphological stability has not been demonstrated sufficiently. For the possible application of such promising particles, it will be very interesting to see if the mass activity can be increased by decreasing the NP size, while retaining high NP stability.

When NPs are used in electrocatalysis, it is of paramount importance that best practices are followed with respect to immobilization, cleaning, and characterization of the NPs on support electrodes. If these aspects are not properly considered, results obtained in different laboratories and experiments are difficult to compare. Additionally, this Review has highlighted that when real catalysts are studied in model environments it is essential to control mass transport and ohmic losses to understand the intrinsic behavior. Mass transport is also a very important consideration when studying model NP ensembles in model environments, particularly for reactions that have soluble intermediates that may readsorb on adjacent NPs, depending on the prevailing mass-transport rate and the interparticle separation.

A major aspect of this Review has been to highlight emerging innovative techniques that hold considerable promise for a breakthrough in understanding the fundamentals of NP electrocatalysis through the study of individual NPs. This type of approach is particularly effective when the activity and structure can be determined and correlated at an individual NP. The main technical challenges are the spatial isolation of a single NP and the measurement of the (often) very low electrochemical current generated at individual NPs. Three techniques were distinguished and discussed. First is the immobilization of individual particles on inert and ultrasmall probes, such as by electrodeposition. The use of this approach to study the ORR revealed how NP size influenced the electrocatalytic activity and the outcome (products) of electrochemical processes.

The second approach is the discrete detection of individual NPs using UMEs. In this case the UME and NP couple is chosen such that the UME is inert to the turnover of a reactant in solution, but it occurs when an NP in solution is polarized upon landing on a UME surface. Several UME/NP combinations have been reported based on this approach, thus indicating that the approach is quite universal. Recently, this approach has been expanded by coupling to other techniques, such as electron microscopy, to allow the direct correlation between structure and activity on a single NP level. Improved quantification and analysis of NP landings are necessary for the further application of this technique, particularly the formulation of more advanced models for NP transport to the support electrode and the interaction of NPs with electrodes.

A final method for elucidating the electrochemistry of individual NPs is the application of probes with a high spatial

resolution, such as scanning nanoelectrodes, scanning droplet cells, and advanced optical measurements, to screen two-dimensional NP ensembles. These measurements have shown heterogeneity in the activity of NPs of apparently similar size, thereby suggesting that minute shape changes can significantly affect the catalytic activity of NPs.

Electrochemical measurements of NPs have now reached a critical phase, in which it has become possible to determine the catalytic activity of NPs in complex membrane electrode assemblies as well as of individual NPs in model environments. The breadth of techniques and the information they provide will aid in the rational design of optimal catalysts for many reactions and greatly advance our understanding of electrochemical processes at the nanoscale.

## Glossary

**{100}, {111}, and {110} planes:** examples of so-called Miller indices that indicate planes of crystal truncation. The catalytic interaction between metal surfaces and reactants depends significantly on the local arrangement of surface atoms of a truncated crystalline solid, which can be referred to by the corresponding Miller index.

**Mass activity:** the catalytic activity (in electrocatalysis expressed as current) normalized by weight of catalyst used. The surface area per weight ratio critically depends on the NP size.

**Nanoscale electrode (NSE):** any electrode with the dominant characteristic dimension smaller than 100 nm.

**ORR/OER/HER/HOR:** commonly discussed electrocatalytic reactions: the oxygen reduction reaction, oxygen evolution reaction, hydrogen evolution reaction, and hydrogen oxidation reaction, respectively; see Section 1.1.

**Proton-exchange membrane (PEM):** usually a polymer (most commonly Nafion) that allows charge-carrier transport between electrodes. These are used as a solid electrolyte in fuel cells.

**Reversible hydrogen electrode (RHE):** the potential of a Pt electrode at which the oxidation of hydrogen gas and the reduction of protons take place in a solution with the same pH value as the working electrolyte, and which occurs reversibly, thus making this system the most suitable reference electrode of choice for electrocatalytic reactions. To be distinguished from the normal hydrogen electrode (NHE), which is the RHE for pH 0.

**Specific activity:** the catalytic activity normalized by the electrochemically active surface area of the catalyst. The electrochemically active surface area can be determined by several methods discussed in Section 2.5.

**Ultramicroelectrode (UME):** electrode with a critical dimension smaller than the characteristic diffusion layer thickness.

**Underpotential deposition (UPD):** electrodeposition of a species at potentials less driving than the equilibrium (Nernst) potential for that process as a result of the strong interaction between the substrate and the species. UPD typically occurs up to a coverage of one monolayer and can thus be used as a probe for the surface area of the substrate.



## Abbreviations

APC	anodic particle coulometry
AFM	atomic force microscopy
CV	cyclic voltammogram
CTAB	cetyltrimethylammonium bromide
DLS	dynamic light scattering
EELS	electron energy loss spectroscopy
ET	electron transfer
fcc	face-centered cubic
HER	hydrogen evolution reaction
HOPG	highly oriented pyrolytic graphite
HOR	hydrogen oxidation reaction
IL-TEM	identical location–transmission electron microscopy
MEA	membrane-electrode assembly
NP	nanoparticle
NSE	nanoscale electrode
NTA	nanoparticle tracking analysis
OER	oxygen evolution reaction
ORR	oxygen reduction reaction
PDMS	polydimethylsiloxane
PPC	pyrolyzed photoresist carbon
PVD	physical vapor deposition
PVP	polyvinylpyrrolidone
QRCE	quasireference counterelectrode
RI	reactive intermediate
RHE	reversible hydrogen electrode
SAM	self-assembled monolayer
SAXS	small-angle X-ray scattering
SECM	scanning electrochemical microscopy
SECCM	scanning electrochemical cell microscopy
SEM	scanning electron microscopy
SPR	surface plasmon resonance
STEM	scanning transmission electron microscopy
STM	scanning tunneling microscopy
TEM	transmission electron microscopy
UME	ultramicroelectrode
UPD	underpotential deposition
XRD	X-ray diffraction
YSZ	yttrium-stabilized zirconia

We gratefully acknowledge financial support from a Marie Curie Intra European Fellowship within FP7 (project 275450 “VISELCAT”) to S.C.S.L., the Netherlands Organisation for Scientific Research (NWO) through a VICI grant awarded to M.T.M.K., and a European Research Council Advanced Investigator Grant (ERC-2009-AdG 247143 “QUANTIF”) to P.R.U.

Received: August 4, 2013

Published online: February 26, 2014

- [1] C. Q. Sun, B. K. Tay, X. T. Zeng, S. Li, T. P. Chen, J. Zhou, H. L. Bai, E. Y. Jiang, *J. Phys. Condens. Matter* **2002**, *14*, 7781–7795.
- [2] D. Zanchet, H. Tolentino, M. C. M. Alves, O. L. Alves, D. Ugarte, *Chem. Phys. Lett.* **2000**, *323*, 167–172.
- [3] A. N. Goldstein, C. M. Echer, A. P. Alivisatos, *Science* **1992**, *256*, 1425–1427.

- [4] M. Haruta, *Chem. Rec.* **2003**, *3*, 75–87.
- [5] M. T. M. Koper, *Nanoscale* **2011**, *3*, 2054–2073.
- [6] Y. Li, E. Boone, M. A. El-Sayed, *Langmuir* **2002**, *18*, 4921–4925.
- [7] S. Link, M. A. El-Sayed, *J. Phys. Chem. B* **1999**, *103*, 4212–4217.
- [8] H. B. Fu, J. N. Yao, *J. Am. Chem. Soc.* **2001**, *123*, 1434–1439.
- [9] B. Zhang, L. Fan, H. Zhong, Y. Liu, S. Chen, *J. Am. Chem. Soc.* **2013**, *135*, 10073–10080.
- [10] J. J. Watkins, H. S. White, *Langmuir* **2004**, *20*, 5474–5483.
- [11] C. P. Smith, H. S. White, *Anal. Chem.* **1993**, *65*, 3343–3353.
- [12] R. He, S. Chen, F. Yang, B. Wu, *J. Phys. Chem. B* **2006**, *110*, 3262–3270.
- [13] A. J. Bard, *J. Am. Chem. Soc.* **2010**, *132*, 7559–7567.
- [14] A. J. Arvia, R. C. Salvarezza, W. E. Triaca, *J. New Mater. Electrochem. Syst.* **2004**, *7*, 133–143.
- [15] F. W. Campbell, R. G. Compton, *Anal. Bioanal. Chem.* **2010**, *396*, 241–259.
- [16] D. Hernández-Santos, M. B. González-García, A. C. García, *Electroanalysis* **2002**, *14*, 1225–1235.
- [17] J. N. Anker, W. P. Hall, O. Lyandres, N. C. Shah, J. Zhao, R. P. Van Duyne, *Nat. Mater.* **2008**, *7*, 442–453.
- [18] S. M. Nie, S. R. Emery, *Science* **1997**, *275*, 1102–1106.
- [19] K. Kneipp, H. Kneipp, I. Itzkan, R. R. Dasari, M. S. Feld, *Chem. Rev.* **1999**, *99*, 2957–2976.
- [20] R. Kitsomboonloha, C. Ngambenjawong, W. S. Mohammed, M. B. Chaudhari, G. L. Hornyak, J. Dutta, *Micro Nano Lett.* **2011**, *6*, 342–344.
- [21] Q. A. Pankhurst, J. Connolly, S. K. Jones, J. Dobson, *J. Phys. D* **2003**, *36*, R167–R181.
- [22] S. M. Moghimi, A. C. Hunter, J. C. Murray, *Pharmacol. Rev.* **2001**, *53*, 283–318.
- [23] B. D. Chithrani, A. A. Ghazani, W. C. W. Chan, *Nano Lett.* **2006**, *6*, 662–668.
- [24] G. K. Wertheim in *Small Particles and Inorganic Clusters* (Eds.: C. Chapon, M. Gillet, C. Henry), Springer, Berlin/Heidelberg, **1989**, pp. 319–326.
- [25] S. Proch, M. Wirth, H. S. White, S. L. Anderson, *J. Am. Chem. Soc.* **2013**, *135*, 3073–3086.
- [26] G. Somorjai, J. Park, *Top. Catal.* **2008**, *49*, 126–135.
- [27] G. Somorjai, Y. Li, *Introduction to Surface Chemistry and Catalysis*, 2 ed., Wiley, Hoboken, **2010**.
- [28] J. K. Nørskov, T. Bligaard, J. Rossmeisl, C. H. Christensen, *Nat. Chem.* **2009**, *1*, 37–46.
- [29] H. A. Gasteiger, S. S. Kocha, B. Sompalli, F. T. Wagner, *Appl. Catal. B* **2005**, *56*, 9–35.
- [30] F. Maillard, S. Pronkin, E. R. Savinova in *Fuel Cell Catalysis: A Surface Science Approach* (Ed.: M. T. M. Koper), Wiley, Hoboken, **2009**.
- [31] R. W. Murray, *Chem. Rev.* **2008**, *108*, 2688–2720.
- [32] S. M. Oja, M. Wood, B. Zhang, *Anal. Chem.* **2013**, *85*, 473–486.
- [33] L. Rassaei, P. S. Singh, S. G. Lemay, *Anal. Chem.* **2011**, *83*, 3974–3980.
- [34] H. Zhang, M. Jin, Y. Xia, *Angew. Chem.* **2012**, *124*, 7774–7792; *Angew. Chem. Int. Ed.* **2012**, *51*, 7656–7673.
- [35] A. Chen, P. Holt-Hindle, *Chem. Rev.* **2010**, *110*, 3767–3804.
- [36] M. Schulze, A. Schneider, E. Gülzow, *J. Power Sources* **2004**, *127*, 213–221.
- [37] K. J. J. Mayrhofer, M. Arenz, B. B. Blizanac, V. Stamenkovic, P. N. Ross, N. M. Markovic, *Electrochim. Acta* **2005**, *50*, 5144–5154.
- [38] S. Chen, A. Kucernak, *J. Phys. Chem. B* **2003**, *107*, 8392–8402.
- [39] M. K. Debe, *Nature* **2012**, *486*, 43–51.
- [40] G. Girishkumar, B. McCloskey, A. C. Luntz, S. Swanson, W. Wilcke, *J. Phys. Chem. Lett.* **2010**, *1*, 2193–2203.
- [41] M. Armand, J. M. Tarascon, *Nature* **2008**, *451*, 652–657.

- [42] V. R. Stamenkovic, B. Fowler, B. S. Mun, G. Wang, P. N. Ross, C. A. Lucas, N. M. Markovic, *Science* **2007**, *315*, 493–497.
- [43] J. K. Nørskov, J. Rossmeisl, A. Logadottir, L. Lindqvist, J. R. Kitchin, T. Bligaard, H. Jónsson, *J. Phys. Chem. B* **2004**, *108*, 17886–17892.
- [44] N. M. Markovic, P. N. Ross, Jr., *Surf. Sci. Rep.* **2002**, *45*, 117–229.
- [45] A. Kuzume, E. Herrero, J. M. Feliu, *J. Electroanal. Chem.* **2007**, *599*, 333–343.
- [46] I. E. L. Stephens, A. S. Bondarenko, U. Grönberg, J. Rossmeisl, I. Chorkendorff, *Energy Environ. Sci.* **2012**, *5*, 6744–6762.
- [47] M. Watanabe, H. Sei, P. Stonehart, *J. Electroanal. Chem.* **1989**, *261*, 375–387.
- [48] Y. E. Seidel, A. Schneider, Z. Jusys, B. Wickman, B. Kasemo, R. J. Behm, *Faraday Discuss.* **2009**, *140*, 167–184.
- [49] S. Chen, A. Kucernak, *J. Phys. Chem. B* **2004**, *108*, 13984–13994.
- [50] A. U. Nilekar, K. Sasaki, C. A. Farberow, R. R. Adzic, M. Mavrikakis, *J. Am. Chem. Soc.* **2011**, *133*, 18574–18576.
- [51] S. M. M. Ehteshami, S. H. Chan, *Electrochim. Acta* **2013**, *93*, 334–345.
- [52] N. P. Brandon, S. Skinner, B. C. H. Steele, *Annu. Rev. Mater. Res.* **2003**, *33*, 183–213.
- [53] Y. Takasu, Y. Fujii, K. Yasuda, Y. Iwanaga, Y. Matsuda, *Electrochim. Acta* **1989**, *34*, 453–458.
- [54] J. Meier, K. A. Friedrich, U. Stimming, *Faraday Discuss.* **2002**, *121*, 365–372.
- [55] V. Rosca, M. T. M. Koper, *Electrochim. Acta* **2008**, *53*, 5199–5205.
- [56] B. Álvarez-Ruiz, R. Gomez, J. M. Orts, J. M. Feliu, *J. Electrochem. Soc.* **2002**, *149*, D35–D45.
- [57] B. E. Hayden, D. Pletcher, J.-P. Suchsland, *Angew. Chem.* **2007**, *119*, 3600–3602; *Angew. Chem. Int. Ed.* **2007**, *46*, 3530–3532.
- [58] B. E. Hayden, D. Pletcher, J.-P. Suchsland, L. J. Williams, *Phys. Chem. Chem. Phys.* **2009**, *11*, 1564–1570.
- [59] B. E. Hayden, D. Pletcher, J.-P. Suchsland, L. J. Williams, *Phys. Chem. Chem. Phys.* **2009**, *11*, 9141–9148.
- [60] M. Haruta, *Catal. Today* **1997**, *36*, 153–166.
- [61] C. T. Campbell, J. C. Sharp, Y. X. Yao, E. M. Karp, T. L. Silbaugh, *Faraday Discuss.* **2011**, *152*, 227–239.
- [62] C. Galeano, R. Güttel, M. Paul, P. Arnal, A.-H. Lu, F. Schüth, *Chem. Eur. J.* **2011**, *17*, 8434–8439.
- [63] A. S. K. Hashmi, G. J. Hutchings, *Angew. Chem.* **2006**, *118*, 8064–8105; *Angew. Chem. Int. Ed.* **2006**, *45*, 7896–7936.
- [64] R. L. McCreery, *Chem. Rev.* **2008**, *108*, 2646–2687.
- [65] L. M. Roen, C. H. Paik, T. D. Jarvic, *Electrochem. Solid-State Lett.* **2004**, *7*, A19–A22.
- [66] P. Serp, M. Corrias, P. Kalck, *Appl. Catal. A* **2003**, *253*, 337–358.
- [67] R. M. Crooks, M. Zhao, L. Sun, V. Chechik, L. K. Yeung, *Acc. Chem. Res.* **2001**, *34*, 181–190.
- [68] G. R. Salazar-Banda, K. I. B. Eguluz, L. A. Avaca, *Electrochem. Commun.* **2007**, *9*, 59–64.
- [69] F. J. Vidal-Iglesias, J. Solla-Gullón, P. Rodríguez, E. Herrero, V. Montiel, J. M. Feliu, A. Aldaz, *Electrochem. Commun.* **2004**, *6*, 1080–1084.
- [70] J. Solla-Gullón, P. Rodríguez, E. Herrero, A. Aldaz, J. M. Feliu, *Phys. Chem. Chem. Phys.* **2008**, *10*, 1359–1373.
- [71] G. Sandmann, H. Dietz, W. Plieth, *J. Electroanal. Chem.* **2000**, *491*, 78–86.
- [72] C. G. Granqvist, A. Hultåker, *Thin Solid Films* **2002**, *411*, 1–5.
- [73] T. Minami, *Semicond. Sci. Technol.* **2005**, *20*, S35–S44.
- [74] R. M. Penner, *J. Phys. Chem. B* **2002**, *106*, 3339–3353.
- [75] M. Bayati, J. M. Abad, R. J. Nichols, D. J. Schiffrin, *J. Phys. Chem. C* **2010**, *114*, 18439–18448.
- [76] B. Scharifker, G. Hills, *Electrochim. Acta* **1983**, *28*, 879–889.
- [77] J. V. Zoval, J. Lee, S. Gorer, R. M. Penner, *J. Phys. Chem. B* **1998**, *102*, 1166–1175.
- [78] H. V. Patten, E. Ventosa, A. Colina, V. Ruiz, J. López-Palacios, A. J. Wain, S. C. S. Lai, J. V. Macpherson, P. R. Unwin, *J. Solid State Electrochem.* **2011**, *15*, 2331–2339.
- [79] T. M. Day, P. R. Unwin, J. V. Macpherson, *Nano Lett.* **2007**, *7*, 51–57.
- [80] T. M. Day, P. R. Unwin, N. R. Wilson, J. V. Macpherson, *J. Am. Chem. Soc.* **2005**, *127*, 10639–10647.
- [81] B. M. Quinn, C. Dekker, S. G. Lemay, *J. Am. Chem. Soc.* **2005**, *127*, 6146–6147.
- [82] B. M. Quinn, S. G. Lemay, *Adv. Mater.* **2006**, *18*, 855–859.
- [83] C. C. Chen, C. S. C. Bose, K. Rajeshwar, *J. Electroanal. Chem.* **1993**, *350*, 161–176.
- [84] M. T. Giacomini, E. A. Ticianelli, J. McBreen, M. Balasubramanian, *J. Electrochem. Soc.* **2001**, *148*, A323–A329.
- [85] R. Schrebler, M. A. del Valle, H. Gómez, C. Veas, R. Córdova, *J. Electroanal. Chem.* **1995**, *380*, 219–227.
- [86] J.-H. Ye, P. S. Fedkiw, *Electrochim. Acta* **1996**, *41*, 221–231.
- [87] G. Kokkinidis, A. Papoutsis, D. Stoychev, A. Milchev, *J. Electroanal. Chem.* **2000**, *486*, 48–55.
- [88] P. Sun, F. Li, C. Yang, T. Sun, I. Kady, B. Hunt, J. Zhuang, *J. Phys. Chem. C* **2013**, *117*, 6120–6125.
- [89] H. Masuda, K. Yasui, K. Nishio, *Adv. Mater.* **2000**, *12*, 1031–1033.
- [90] A. R. Howells, L. Hung, G. S. Chottiner, D. A. Scherson, *Solid State Ionics* **2002**, *150*, 53–62.
- [91] K. L. Yeung, E. E. Wolf, *J. Vac. Sci. Technol. A* **1992**, *10*, 651–656.
- [92] C. R. Henry, *Surf. Sci. Rep.* **1998**, *31*, 231–325.
- [93] K. Yahikozawa, Y. Fujii, Y. Matsuda, K. Nishimura, Y. Takasu, *Electrochim. Acta* **1991**, *36*, 973–978.
- [94] N. Tian, Z.-Y. Zhou, S.-G. Sun, Y. Ding, Z. L. Wang, *Science* **2007**, *316*, 732–735.
- [95] J. Ustarroz, U. Gupta, A. Hubin, S. Bals, H. Terryn, *Electrochem. Commun.* **2010**, *12*, 1706–1709.
- [96] D. Zhang, W. C. Chang, T. Okajima, T. Ohsaka, *Langmuir* **2011**, *27*, 14662–14668.
- [97] J. Ustarroz, X. Ke, A. Hubin, S. Bals, H. Terryn, *J. Phys. Chem. C* **2012**, *116*, 2322–2329.
- [98] M. J. Williamson, R. M. Tromp, P. M. Vereecken, R. Hull, F. M. Ross, *Nat. Mater.* **2003**, *2*, 532–536.
- [99] A. Radisic, P. M. Vereecken, J. B. Hannon, P. C. Searson, F. M. Ross, *Nano Lett.* **2006**, *6*, 238–242.
- [100] J. Ustarroz, J. A. Hammons, Y. Van Ingelgem, M. Tzedaki, A. Hubin, H. Terryn, *Electrochem. Commun.* **2011**, *13*, 1320–1323.
- [101] E. Garcia-Pastoriza, J. Mostany, B. R. Scharifker, *J. Electroanal. Chem.* **1998**, *441*, 13–18.
- [102] P. V. Dudin, P. R. Unwin, J. V. Macpherson, *J. Phys. Chem. C* **2010**, *114*, 13241–13248.
- [103] P. L. Redmond, A. J. Hallock, L. E. Brus, *Nano Lett.* **2005**, *5*, 131–135.
- [104] H. Liu, R. M. Penner, *J. Phys. Chem. B* **2000**, *104*, 9131–9139.
- [105] H. Liu, F. Favier, K. Ng, M. P. Zach, R. M. Penner, *Electrochim. Acta* **2001**, *47*, 671–677.
- [106] W. Plieth, H. Dietz, G. Sandmann, A. Meixner, M. Weber, P. Moyer, J. Schmidt, *Electrochim. Acta* **1999**, *44*, 3659–3666.
- [107] M. Bayati, J. M. Abad, C. A. Bridges, M. J. Rosseinsky, D. J. Schiffrin, *J. Electroanal. Chem.* **2008**, *623*, 19–28.
- [108] T. Brülle, A. Denisenko, H. Sternschulte, U. Stimming, *Phys. Chem. Chem. Phys.* **2011**, *13*, 12883–12891.
- [109] T. Brülle, W. Ju, P. Niedermayr, A. Denisenko, O. Paschos, O. Schneider, U. Stimming, *Molecules* **2011**, *16*, 10059–10077.
- [110] M. P. Zach, R. M. Penner, *Adv. Mater.* **2000**, *12*, 878–883.
- [111] S. C. S. Lai, P. V. Dudin, J. V. Macpherson, P. R. Unwin, *J. Am. Chem. Soc.* **2011**, *133*, 10744–10747.

- [112] J. L. Fransaer, R. M. Penner, *J. Phys. Chem. B* **1999**, *103*, 7643–7653.
- [113] J. Dai, M. L. Bruening, *Nano Lett.* **2002**, *2*, 497–501.
- [114] S. Joly, R. Kane, L. Radzilowski, T. Wang, A. Wu, R. E. Cohen, E. L. Thomas, M. F. Rubner, *Langmuir* **2000**, *16*, 1354–1359.
- [115] S. Dante, Z. Hou, S. Risbud, P. Stroeve, *Langmuir* **1999**, *15*, 2176–2182.
- [116] X. Shi, M. Shen, H. Möhwald, *Prog. Polym. Sci.* **2004**, *29*, 987–1019.
- [117] X. Zhang, Z. Su, *Adv. Mater.* **2012**, *24*, 4574–4577.
- [118] P. Bertinello, M. Peruffo, P. R. Unwin, *Chem. Commun.* **2007**, 1597–1599.
- [119] P. Allongue, M. Delamar, B. Desbat, O. Fagebaume, R. Hitmi, J. Pinson, J.-M. Savéant, *J. Am. Chem. Soc.* **1997**, *119*, 201–207.
- [120] M. Delamar, R. Hitmi, J. Pinson, J. M. Saveant, *J. Am. Chem. Soc.* **1992**, *114*, 5883–5884.
- [121] A. J. Downard, *Electroanalysis* **2000**, *12*, 1085–1096.
- [122] J. Pinson, F. Podvorica, *Chem. Soc. Rev.* **2005**, *34*, 429–439.
- [123] S. Mahouche-Chergui, S. Gam-Derouich, C. Mangeney, M. M. Chehimi, *Chem. Soc. Rev.* **2011**, *40*, 4143–4166.
- [124] M. M. Waje, X. Wang, W. Li, Y. Yan, *Nanotechnology* **2005**, *16*, S395–400.
- [125] D.-J. Guo, H.-L. Li, *Electrochem. Commun.* **2004**, *6*, 999–1003.
- [126] D. J. Guo, H. L. Li, *Carbon* **2005**, *43*, 1259–1264.
- [127] J. Turkevich, P. C. Stevenson, J. Hillier, *Discuss. Faraday Soc.* **1951**, *11*, 55–75.
- [128] M. Brust, M. Walker, D. Bethell, D. J. Schiffrin, R. Whyman, *J. Chem. Soc. Chem. Commun.* **1994**, 801–802.
- [129] B. L. Cushing, V. L. Kolesnichenko, C. J. O'Connor, *Chem. Rev.* **2004**, *104*, 3893–3946.
- [130] R. Van Hardeveld, F. Hartog, *Surf. Sci.* **1969**, *15*, 189–230.
- [131] Y. Xia, Y. Xiong, B. Lim, S. E. Skrabalak, *Angew. Chem.* **2009**, *121*, 62–108; *Angew. Chem. Int. Ed.* **2009**, *48*, 60–103.
- [132] T. K. Sau, A. L. Rogach, *Adv. Mater.* **2010**, *22*, 1781–1804.
- [133] K. Zhou, Y. Li, *Angew. Chem.* **2012**, *124*, 622–635; *Angew. Chem. Int. Ed.* **2012**, *51*, 602–613.
- [134] Y. Niu, R. M. Crooks, *C. R. Chim.* **2003**, *6*, 1049–1059.
- [135] F. Gröhn, B. J. Bauer, Y. A. Akpalu, C. L. Jackson, E. J. Amis, *Macromolecules* **2000**, *33*, 6042–6050.
- [136] K. Esumi, A. Suzuki, A. Yamahira, K. Torigoe, *Langmuir* **2000**, *16*, 2604–2608.
- [137] M. Q. Zhao, R. M. Crooks, *Angew. Chem.* **1999**, *111*, 375–377; *Angew. Chem. Int. Ed.* **1999**, *38*, 364–366.
- [138] M. Q. Zhao, R. M. Crooks, *Adv. Mater.* **1999**, *11*, 217–220.
- [139] M. Q. Zhao, L. Sun, R. M. Crooks, *J. Am. Chem. Soc.* **1998**, *120*, 4877–4878.
- [140] R. W. J. Scott, O. M. Wilson, R. M. Crooks, *J. Phys. Chem. B* **2005**, *109*, 692–704.
- [141] F. Aulenta, W. Hayes, S. Rannard, *Eur. Polym. J.* **2003**, *39*, 1741–1771.
- [142] F. Vögtle, S. Gestermann, R. Hesse, H. Schwierz, B. Windisch, *Prog. Polym. Sci.* **2000**, *25*, 987–1041.
- [143] H. Ye, R. M. Crooks, *J. Am. Chem. Soc.* **2005**, *127*, 4930–4934.
- [144] A. I. Yanson, P. Rodriguez, N. Garcia-Araez, R. V. Mom, F. D. Tichelaar, M. T. M. Koper, *Angew. Chem.* **2011**, *123*, 6470–6474; *Angew. Chem. Int. Ed.* **2011**, *50*, 6346–6350.
- [145] P. Rodriguez, F. D. Tichelaar, M. T. M. Koper, A. I. Yanson, *J. Am. Chem. Soc.* **2011**, *133*, 17626–17629.
- [146] A. I. Yanson, P. V. Antonov, Y. I. Yanson, M. T. M. Koper, *Electrochim. Acta* **2013**, *110*, 796–800.
- [147] A. I. Yanson, P. V. Antonov, P. Rodriguez, M. T. M. Koper, *Electrochim. Acta* **2013**, *110*, 913–918.
- [148] R. D. Deegan, O. Bakajin, T. F. Dupont, G. Huber, S. R. Nagel, T. A. Witten, *Nature* **1997**, *389*, 827–829.
- [149] T. A. H. Nguyen, M. A. Hampton, A. V. Nguyen, *J. Phys. Chem. C* **2013**, *117*, 4707–4716.
- [150] M. A. Hampton, T. A. H. Nguyen, A. V. Nguyen, Z. P. Xu, L. Huang, V. Rudolph, *J. Colloid Interface Sci.* **2012**, *377*, 456–462.
- [151] R. G. Freeman, K. C. Grabar, K. J. Allison, R. M. Bright, J. A. Davis, A. P. Guthrie, M. B. Hommer, M. A. Jackson, P. C. Smith, D. G. Walter, M. J. Natan, *Science* **1995**, *267*, 1629–1632.
- [152] W. Cheng, S. Dong, E. Wang, *Angew. Chem.* **2003**, *115*, 465–468; *Angew. Chem. Int. Ed.* **2003**, *42*, 449–452.
- [153] W. Cheng, S. Dong, E. Wang, *J. Phys. Chem. B* **2004**, *108*, 19146–19154.
- [154] Y. X. Li, J. T. Cox, B. Zhang, *J. Am. Chem. Soc.* **2010**, *132*, 3047–3054.
- [155] T. Zhu, X. Fu, T. Mu, J. Wang, Z. Liu, *Langmuir* **1999**, *15*, 5197–5199.
- [156] C. A. Goss, D. H. Charych, M. Majda, *Anal. Chem.* **1991**, *63*, 85–88.
- [157] Y. Tang, W. Cheng, *Langmuir* **2013**, *29*, 3125–3132.
- [158] K. C. Grabar, P. C. Smith, M. D. Musick, J. A. Davis, D. G. Walter, M. A. Jackson, A. P. Guthrie, M. J. Natan, *J. Am. Chem. Soc.* **1996**, *118*, 1148–1153.
- [159] K. C. Grabar, K. J. Allison, B. E. Baker, R. M. Bright, K. R. Brown, R. G. Freeman, A. P. Fox, C. D. Keating, M. D. Musick, M. J. Natan, *Langmuir* **1996**, *12*, 2353–2361.
- [160] W. Cheng, S. Dong, E. Wang, *Langmuir* **2002**, *18*, 9947–9952.
- [161] S. L. Horswell, I. A. O'Neil, D. J. Schiffrin, *J. Phys. Chem. B* **2003**, *107*, 4844–4854.
- [162] B. K. Jena, S. J. Percival, B. Zhang, *Anal. Chem.* **2010**, *82*, 6737–6743.
- [163] D. Bethell, M. Brust, D. J. Schiffrin, C. Kiely, *J. Electroanal. Chem.* **1996**, *409*, 137–143.
- [164] M. Brust, D. Bethell, C. J. Kiely, D. J. Schiffrin, *Langmuir* **1998**, *14*, 5425–5429.
- [165] C. R. Bradbury, J. Zhao, D. J. Fermín, *J. Phys. Chem. C* **2008**, *112*, 10153–10160.
- [166] J. Zhao, C. R. Bradbury, D. J. Fermín, *J. Phys. Chem. C* **2008**, *112*, 6832–6841.
- [167] J. B. Shein, L. M. H. Lai, P. K. Eggers, M. N. Paddon-Row, J. J. Gooding, *Langmuir* **2009**, *25*, 11121–11128.
- [168] J. Guo, C.-N. Ho, P. Sun, *Electroanalysis* **2011**, *23*, 481–486.
- [169] D. K. Schwartz, *Annu. Rev. Phys. Chem.* **2001**, *52*, 107–137.
- [170] J. J. Gooding, F. Mearns, W. Yang, J. Liu, *Electroanalysis* **2003**, *15*, 81–96.
- [171] A. Ulman, *Chem. Rev.* **1996**, *96*, 1533–1554.
- [172] J. C. Love, L. A. Estroff, J. K. Kriebel, R. G. Nuzzo, G. M. Whitesides, *Chem. Rev.* **2005**, *105*, 1103–1170.
- [173] F. Schreiber, *Prog. Surf. Sci.* **2000**, *65*, 151–257.
- [174] G. Le Saux, S. Ciampi, K. Gaus, J. J. Gooding, *ACS Appl. Mater. Interfaces* **2009**, *1*, 2477–2483.
- [175] M.-C. Chuang, J.-a. A. Ho, *RSC Adv.* **2012**, *2*, 4092–4096.
- [176] D. M. Adams, L. Brus, C. E. D. Chidsey, S. Creager, C. Creutz, C. R. Kagan, P. V. Kamat, M. Lieberman, S. Lindsay, R. A. Marcus, R. M. Metzger, M. E. Michel-Beyerle, J. R. Miller, M. D. Newton, D. R. Rolison, O. Sankey, K. S. Schanze, J. Yardley, X. Zhu, *J. Phys. Chem. B* **2003**, *107*, 6668–6697.
- [177] A. Chou, P. K. Eggers, M. N. Paddon-Row, J. J. Gooding, *J. Phys. Chem. C* **2009**, *113*, 3203–3211.
- [178] M. N. Paddon-Row, *Acc. Chem. Res.* **1994**, *27*, 18–25.
- [179] D. J. Wold, C. D. Frisbie, *J. Am. Chem. Soc.* **2001**, *123*, 5549–5556.
- [180] A. Barfidokht, S. Ciampi, E. Luais, N. Darwish, J. J. Gooding, *Anal. Chem.* **2013**, *85*, 1073–1080.
- [181] W. Cheng, S. Dong, E. Wang, *Anal. Chem.* **2002**, *74*, 3599–3604.
- [182] J. Zhao, M. Wasem, C. R. Bradbury, D. J. Fermín, *J. Phys. Chem. C* **2008**, *112*, 7284–7289.
- [183] J. N. Chazalviel, P. Allongue, *J. Am. Chem. Soc.* **2011**, *133*, 762–764.



- [184] J. N. Kuhn, C.-K. Tsung, W. Huang, G. A. Somorjai, *J. Catal.* **2009**, 265, 209–215.
- [185] J. Solla-Gullón, V. Montiel, A. Aldaz, J. Clavilier, *J. Electroanal. Chem.* **2000**, 491, 69–77.
- [186] H.-X. Zhang, H. Wang, Y.-S. Re, W.-B. Cai, *Chem. Commun.* **2012**, 48, 8362–8364.
- [187] J. Monzó, M. T. M. Koper, P. Rodriguez, *ChemPhysChem* **2012**, 13, 709–715.
- [188] F. J. Vidal-Iglesias, J. Solla-Gullón, E. Herrero, V. Montiel, A. Aldaz, J. M. Feliu, *Electrochem. Commun.* **2011**, 13, 502–505.
- [189] C. Aliaga, J. Y. Park, Y. Yamada, H. S. Lee, C.-K. Tsung, P. Yang, G. A. Somorjai, *J. Phys. Chem. C* **2009**, 113, 6150–6155.
- [190] J. Clavilier, R. Faure, G. Guinet, R. Durand, *J. Electroanal. Chem.* **1979**, 107, 205–209.
- [191] J. Clavilier, D. Armand, *J. Electroanal. Chem.* **1986**, 199, 187–200.
- [192] S. Trasatti, O. A. Petrii, *Pure Appl. Chem.* **1991**, 63, 711–734.
- [193] F. J. Vidal-Iglesias, R. M. Arán-Ais, J. Solla-Gullón, E. Herrero, J. M. Feliu, *ACS Catal.* **2012**, 2, 901–910.
- [194] J. Hernández, J. Solla-Gullón, E. Herrero, A. Aldaz, J. M. Feliu, *J. Phys. Chem. C* **2007**, 111, 14078–14083.
- [195] C. L. Green, A. Kucernak, *J. Phys. Chem. B* **2002**, 106, 1036–1047.
- [196] K. J. J. Mayrhofer, D. Strmcnik, B. B. Bliznac, V. Stamenkovic, M. Arenz, N. M. Markovic, *Electrochim. Acta* **2008**, 53, 3181–3188.
- [197] P. Ochal, J. L. Gomez de La Fuente, M. Tsyppkin, F. Seland, S. Sunde, N. Muthuswamy, M. Rønning, D. Chen, S. Garcia, S. Alayoglu, B. Eichhorn, *J. Electroanal. Chem.* **2011**, 655, 140–146.
- [198] T. Vidaković, M. Christov, K. Sundmacher, *Electrochim. Acta* **2007**, 52, 5606–5613.
- [199] T. H. M. Housmans, J. M. Feliu, M. T. M. Koper, *J. Electroanal. Chem.* **2004**, 572, 79–91.
- [200] J. Grobelny, F. W. DelRio, N. Pradeep, D.-I. Kim, V. A. Hackley, R. F. Cook in *Methods in Molecular Biology*, Vol. 697 (Ed.: J. M. Walker), **2009**, pp. 71–82.
- [201] H. Borchert, E. V. Shevchenko, A. Robert, I. Mekis, A. Kornowski, G. Gruebel, H. Weller, *Langmuir* **2005**, 21, 1931–1936.
- [202] X. Liu, Q. Dai, L. Austin, J. Coutts, G. Knowles, J. Zou, H. Chen, Q. Huo, *J. Am. Chem. Soc.* **2008**, 130, 2780–2782.
- [203] V. Filipe, A. Hawe, W. Jiskoot, *Pharm. Res.* **2010**, 27, 796–810.
- [204] M. Kerker, *The Scattering of Light and Other Electromagnetic Radiation*, Academic Press, London, **1969**.
- [205] V. Amendola, M. Meneghetti, *J. Mater. Chem.* **2007**, 17, 4705–4710.
- [206] V. Amendola, S. Polizzi, M. Meneghetti, *Langmuir* **2007**, 23, 6766–6770.
- [207] Z. L. Wang, *J. Phys. Chem. B* **2000**, 104, 1153–1175.
- [208] J. Ustarroz, J. A. Hammons, T. Altantzis, A. Hubin, S. Bals, H. Terryn, *J. Am. Chem. Soc.* **2013**, 135, 11550–11561.
- [209] Y. E. Seidel, Z. Jusys, B. Wickman, B. Kasemo, R. J. Behm, *ECS Trans.* **2010**, 25, 91–102.
- [210] M. C. Henstridge, R. G. Compton, *Chem. Rec.* **2012**, 12, 63–71.
- [211] J. Guo, E. Lindner, *Anal. Chem.* **2009**, 81, 130–138.
- [212] N. C. Rudd, S. Cannan, E. Bitziou, I. Ciani, A. L. Whitworth, P. R. Unwin, *Anal. Chem.* **2005**, 77, 6205–6217.
- [213] M. Gustavsson, H. Fredriksson, B. Kasemo, Z. Jusys, J. Kaiser, C. Jun, R. J. Behm, *J. Electroanal. Chem.* **2004**, 568, 371–377.
- [214] R. G. Compton, P. R. Unwin, *J. Electroanal. Chem.* **1986**, 205, 1–20.
- [215] Y. E. Seidel, A. Schneider, Z. Jusys, B. Wickman, B. Kasemo, R. J. Behm, *Langmuir* **2010**, 26, 3569–3578.
- [216] I. Dumitrescu, D. F. Yancey, R. M. Crooks, *Lab Chip* **2012**, 12, 986–993.
- [217] I. Dumitrescu, R. M. Crooks, *Proc. Natl. Acad. Sci. USA* **2012**, 109, 11493–11497.
- [218] S. Amemiya, A. J. Bard, F. R. F. Fan, M. V. Mirkin, P. R. Unwin, *Annu. Rev. Anal. Chem.* **2008**, 1, 95–131.
- [219] S. C. S. Lai, J. V. Macpherson, P. R. Unwin, *MRS Bull.* **2012**, 37, 668–674.
- [220] J. L. Fernández, D. A. Walsh, A. J. Bard, *J. Am. Chem. Soc.* **2005**, 127, 357–365.
- [221] S. Jayaraman, A. C. Hillier, *J. Phys. Chem. B* **2003**, 107, 5221–5230.
- [222] A. Minguzzi, M. A. Alpuche-Aviles, J. R. López, S. Rondinini, A. J. Bard, *Anal. Chem.* **2008**, 80, 4055–4064.
- [223] C. M. Sánchez-Sánchez, A. J. Bard, *Anal. Chem.* **2009**, 81, 8094–8100.
- [224] G. Lu, J. S. Cooper, P. J. McGinn, *J. Power Sources* **2006**, 161, 106–114.
- [225] M. V. Mirkin, W. Nogala, J. Velmurugan, Y. Wang, *Phys. Chem. Chem. Phys.* **2011**, 13, 21196–21212.
- [226] J. Zhang, R. M. Lahtinen, K. Kontturi, P. R. Unwin, D. J. Schiffrin, *Chem. Commun.* **2001**, 1818–1819.
- [227] F. Li, I. Ciani, P. Bertocello, P. R. Unwin, J. Zhao, C. R. Bradbury, D. J. Fermín, *J. Phys. Chem. C* **2008**, 112, 9686–9694.
- [228] B. E. Hayden, *Acc. Chem. Res.* **2013**, 46, 1858–1866.
- [229] S. Guerin, B. E. Hayden, *J. Comb. Chem.* **2006**, 8, 66–73.
- [230] S. Guerin, B. E. Hayden, D. Pletcher, M. E. Rendall, J.-P. Suchsland, L. J. Williams, *J. Comb. Chem.* **2006**, 8, 791–798.
- [231] J. C. Meier, I. Katsounaros, C. Galeano, H. J. Bongard, A. A. Topalov, A. Kostka, A. Karschin, F. Schuth, K. J. J. Mayrhofer, *Energy Environ. Sci.* **2012**, 5, 9319–9330.
- [232] K. J. J. Mayrhofer, J. C. Meier, S. J. Ashton, G. K. H. Wiberg, F. Kraus, M. Hanzlik, M. Arenz, *Electrochem. Commun.* **2008**, 10, 1144–1147.
- [233] H. L. Xin, J. A. Mundy, Z. Liu, R. Cabezas, R. Hovden, L. F. Kourkoutis, J. Zhang, N. P. Subramanian, R. Makharia, F. T. Wagner, D. A. Muller, *Nano Lett.* **2012**, 12, 490–497.
- [234] Y. Yu, H. L. Xin, R. Hovden, D. Wang, E. D. Rus, J. A. Mundy, D. A. Muller, H. D. Abruña, *Nano Lett.* **2012**, 12, 4417–4423.
- [235] E. Endoh, S. Terazono, H. Widjaja, Y. Takimoto, *Electrochem. Solid-State Lett.* **2004**, 7, A209–A211.
- [236] A. Taniguchi, T. Akita, K. Yasuda, Y. Miyazaki, *J. Power Sources* **2004**, 130, 42–49.
- [237] T. S. Ahmadi, Z. L. Wang, T. C. Green, A. Henglein, M. A. El-Sayed, *Science* **1996**, 272, 1924–1926.
- [238] T. S. Ahmadi, Z. L. Wang, A. Henglein, M. A. El-Sayed, *Chem. Mater.* **1996**, 8, 1161–1163.
- [239] M. Chen, B. Wu, J. Yang, N. Zheng, *Adv. Mater.* **2012**, 24, 862–879.
- [240] C. Burda, X. Chen, R. Narayanan, M. A. El-Sayed, *Chem. Rev.* **2005**, 105, 1025–1102.
- [241] R. Narayanan, M. A. El-Sayed, *J. Phys. Chem. B* **2005**, 109, 12663–12676.
- [242] M. Grzelczak, J. Perez-Juste, P. Mulvaney, L. M. Liz-Marzan, *Chem. Soc. Rev.* **2008**, 37, 1783–1791.
- [243] S. Guo, E. Wang, *Nano Today* **2011**, 6, 240–264.
- [244] A. R. Tao, S. Habas, P. D. Yang, *Small* **2008**, 4, 310–325.
- [245] Z. M. Peng, H. Yang, *Nano Today* **2009**, 4, 143–164.
- [246] F. J. Vidal-Iglesias, N. Garcia-Arárez, V. Montiel, J. M. Feliu, A. Aldaz, *Electrochem. Commun.* **2003**, 5, 22–26.
- [247] F. J. Vidal-Iglesias, R. M. Arán-Ais, J. Solla-Gullón, E. Garnier, E. Herrero, A. Aldaz, J. M. Feliu, *Phys. Chem. Chem. Phys.* **2012**, 14, 10258–10265.
- [248] V. Grozovski, J. Solla-Gullón, V. Climent, E. Herrero, J. M. Feliu, *J. Phys. Chem. C* **2010**, 114, 13802–13812.
- [249] C. Wang, H. Daimon, Y. Lee, J. Kim, S. Sun, *J. Am. Chem. Soc.* **2007**, 129, 6974–6975.



- [250] Y. Kang, M. Li, Y. Cai, M. Cargnello, R. E. Diaz, T. R. Gordon, N. L. Wieder, R. R. Adzic, R. J. Gorte, E. A. Stach, C. B. Murray, *J. Am. Chem. Soc.* **2013**, *135*, 2741–2747.
- [251] L. Lu, G. Yin, Z. Wang, Y. Gao, *Electrochem. Commun.* **2009**, *11*, 1596–1598.
- [252] C. Wang, H. Daimon, T. Onodera, T. Koda, S. Sun, *Angew. Chem.* **2008**, *120*, 3644–3647; *Angew. Chem. Int. Ed.* **2008**, *47*, 3588–3591.
- [253] M. Rodríguez-López, J. Solla-Gullón, E. Herrero, P. Tuñón, J. M. Feliu, A. Aldaz, A. Carrasquillo, *J. Am. Chem. Soc.* **2010**, *132*, 2233–2242.
- [254] C. M. Sánchez-Sánchez, F. J. Vidal-Iglesias, J. Solla-Gullón, V. Montiel, A. Aldaz, J. M. Feliu, E. Herrero, *Electrochim. Acta* **2010**, *55*, 8252–8257.
- [255] V. Bansal, V. Li, A. P. O'Mullane, S. K. Bhargava, *CrystEngComm* **2010**, *12*, 4280–4286.
- [256] M. Duca, P. Rodríguez, A. I. Yanson, M. T. M. Koper, *Top. Catal.* **2014**, *57*, 255–264.
- [257] Z.-Y. Zhou, N. Tian, J.-T. Li, I. Broadwell, S.-G. Sun, *Chem. Soc. Rev.* **2011**, *40*, 4167–4185.
- [258] Y. Ding, Y. Gao, Z. L. Wanga, N. Tian, Z. Y. Zhou, S. G. Sun, *Appl. Phys. Lett.* **2007**, *91*, 121901.
- [259] Z.-Y. Zhou, Z.-Z. Huang, D.-J. Chen, Q. Wang, N. Tian, S.-G. Sun, *Angew. Chem.* **2010**, *122*, 421–424; *Angew. Chem. Int. Ed.* **2010**, *49*, 411–414.
- [260] Y.-J. Deng, N. Tian, Z.-Y. Zhou, R. Huang, Z.-L. Liu, J. Xiao, S.-G. Sun, *Chem. Sci.* **2012**, *3*, 1157–1161.
- [261] N. Tian, Z.-Y. Zhou, N.-F. Yu, L.-Y. Wang, S.-G. Sun, *J. Am. Chem. Soc.* **2010**, *132*, 7580–7581.
- [262] Z.-Y. Zhou, S.-J. Shang, N. Tian, B.-H. Wu, N.-F. Zheng, B.-B. Xu, C. Chen, H.-H. Wang, D.-M. Xiang, S.-G. Sun, *Electrochem. Commun.* **2012**, *22*, 61–64.
- [263] N. Tian, J. Xiao, Z.-Y. Zhou, H.-X. Liu, Y.-J. Deng, L. Huang, B.-B. Xu, S.-G. Sun, *Faraday Discuss.* **2013**, *162*, 77–89.
- [264] Z. Y. Zhou, N. Tian, Z. Z. Huang, D. J. Chen, S. G. Sun, *Faraday Discuss.* **2009**, *140*, 81–92.
- [265] N. Tian, Z.-Y. Zhou, S.-G. Sun, *Chem. Commun.* **2009**, 1502–1504.
- [266] Q. Cheng, Y.-X. Jiang, N. Tian, Z.-Y. Zhou, S.-G. Sun, *Electrochim. Acta* **2010**, *55*, 8273–8279.
- [267] Y.-X. Chen, S.-P. Chen, Z.-Y. Zhou, N. Tian, Y.-X. Jiang, S.-G. Sun, Y. Ding, Z. L. Wang, *J. Am. Chem. Soc.* **2009**, *131*, 10860–10862.
- [268] Q.-S. Chen, Z.-Y. Zhou, F. J. Vidal-Iglesias, J. Solla-Gullón, J. M. Feliu, S.-G. Sun, *J. Am. Chem. Soc.* **2011**, *133*, 12930–12933.
- [269] H.-X. Liu, N. Tian, M. P. Brandon, J. Pei, Z.-C. Huangfu, C. Zhan, Z.-Y. Zhou, C. Hardacre, W.-F. Lin, S.-G. Sun, *Phys. Chem. Chem. Phys.* **2012**, *14*, 16415–16423.
- [270] H.-X. Liu, N. Tian, M. P. Brandon, Z.-Y. Zhou, J.-L. Lin, C. Hardacre, W.-F. Lin, S.-G. Sun, *ACS Catal.* **2012**, *2*, 708–715.
- [271] R. Huang, Y.-H. Wen, Z.-Z. Zhu, S.-G. Sun, *J. Mater. Chem.* **2011**, *21*, 11578–11584.
- [272] Y. Wen, H. Fang, Z. Zhu, S. Sun, *Phys. Lett. A* **2009**, *373*, 272–276.
- [273] Y.-H. Wen, H. Fang, Z.-Z. Zhu, S.-G. Sun, *Chem. Phys. Lett.* **2009**, *471*, 295–299.
- [274] S. Cherevko, A. A. Topalov, I. Katsounaros, K. J. J. Mayrhofer, *Electrochem. Commun.* **2013**, *28*, 44–46.
- [275] A. A. Topalov, I. Katsounaros, M. Auinger, S. Cherevko, J. C. Meier, S. O. Klemm, K. J. J. Mayrhofer, *Angew. Chem.* **2012**, *124*, 12782–12785; *Angew. Chem. Int. Ed.* **2012**, *51*, 12613–12615.
- [276] J. T. Cox, B. Zhang, *Annu. Rev. Anal. Chem.* **2012**, *5*, 253–272.
- [277] C. J. Slevin, N. J. Gray, J. V. Macpherson, M. A. Webb, P. R. Unwin, *Electrochem. Commun.* **1999**, *1*, 282–288.
- [278] J. L. Conyers, H. S. White, *Anal. Chem.* **2000**, *72*, 4441–4446.
- [279] P. Sun, M. V. Mirkin, *Anal. Chem.* **2006**, *78*, 6526–6534.
- [280] R. M. Penner, M. J. Heben, T. L. Longin, N. S. Lewis, *Science* **1990**, *250*, 1118–1121.
- [281] G. P. Kittleson, H. S. White, M. S. Wrighton, *J. Am. Chem. Soc.* **1984**, *106*, 7389–7396.
- [282] O. Ordeig, C. E. Banks, T. J. Davies, J. del Campo, R. Mas, F. X. Munoz, R. G. Compton, *Analyst* **2006**, *131*, 440–445.
- [283] S. E. F. Kleijn, A. I. Yanson, M. T. M. Koper, *J. Electroanal. Chem.* **2012**, *666*, 19–24.
- [284] F. J. M. Hoebe, F. S. Meijer, C. Dekker, S. P. J. Albracht, H. A. Heering, S. G. Lemay, *ACS Nano* **2008**, *2*, 2497–2504.
- [285] D. Krapf, M.-Y. Wu, R. M. M. Smeets, H. W. Zandbergen, C. Dekker, S. G. Lemay, *Nano Lett.* **2006**, *6*, 105–109.
- [286] G. Mészáros, C. Li, I. Pobelov, T. Wandlowski, *Nanotechnology* **2007**, *18*, 424004.
- [287] G. Mészáros, S. Kronholz, S. Karthäuser, D. Mayer, T. Wandlowski, *Appl. Phys. A* **2007**, *87*, 569–575.
- [288] N. Ebejer, M. Schnipper, A. W. Colburn, M. A. Edwards, P. R. Unwin, *Anal. Chem.* **2010**, *82*, 9141–9145.
- [289] M. E. Snowden, A. G. Güell, S. C. S. Lai, K. McKelvey, N. Ebejer, M. A. O'Connell, A. W. Colburn, P. R. Unwin, *Anal. Chem.* **2012**, *84*, 2483–2491.
- [290] A. G. Güell, N. Ebejer, M. E. Snowden, K. McKelvey, J. V. Macpherson, P. R. Unwin, *Proc. Natl. Acad. Sci. USA* **2012**, *109*, 11487–11492.
- [291] A. G. Güell, N. Ebejer, M. E. Snowden, J. V. Macpherson, P. R. Unwin, *J. Am. Chem. Soc.* **2012**, *134*, 7258–7261.
- [292] S. C. S. Lai, A. N. Patel, K. McKelvey, P. R. Unwin, *Angew. Chem.* **2012**, *124*, 5501–5504; *Angew. Chem. Int. Ed.* **2012**, *51*, 5405–5408.
- [293] H. V. Patten, S. C. S. Lai, J. V. Macpherson, P. R. Unwin, *Anal. Chem.* **2012**, *84*, 5427–5432.
- [294] S. E. F. Kleijn, S. C. S. Lai, T. S. Miller, A. I. Yanson, M. T. M. Koper, P. R. Unwin, *J. Am. Chem. Soc.* **2012**, *134*, 18558–18561.
- [295] A. N. Patel, M. G. Collignon, M. A. O'Connell, W. O. Y. Hung, K. McKelvey, J. V. Macpherson, P. R. Unwin, *J. Am. Chem. Soc.* **2012**, *134*, 20117–20130.
- [296] A. N. Patel, K. McKelvey, P. R. Unwin, *J. Am. Chem. Soc.* **2012**, *134*, 20246–20249.
- [297] B. D. B. Aaronson, C.-H. Chen, H. Li, M. T. M. Koper, S. C. S. Lai, P. R. Unwin, *J. Am. Chem. Soc.* **2013**, *135*, 3873–3880.
- [298] N. Ebejer, A. G. Güell, S. C. S. Lai, K. McKelvey, M. E. Snowden, P. R. Unwin, *Annu. Rev. Anal. Chem.* **2013**, *6*, 329–351.
- [299] M. M. Lohrengel, A. Moehring, M. Pilaski, *Electrochim. Acta* **2001**, *47*, 137–141.
- [300] C. G. Williams, M. A. Edwards, A. L. Colley, J. V. Macpherson, P. R. Unwin, *Anal. Chem.* **2009**, *81*, 2486–2495.
- [301] T. Suter, H. Böhm, *Electrochim. Acta* **1997**, *42*, 3275–3280.
- [302] J. W. Schultze, M. Pilaski, M. M. Lohrengel, U. König, *Faraday Discuss.* **2002**, *121*, 211–227.
- [303] F. Cortés-Salazar, A. Lesch, D. Momotenko, J.-M. Busnel, G. Wittstock, H. H. Girault, *Anal. Methods* **2010**, *2*, 817–823.
- [304] M. Carminati, G. Ferrari, D. Bianchi, M. Sampietro, *Electrochim. Acta* **2013**, *112*, 950–956.
- [305] J. J. Watkins, J. Chen, H. S. White, H. D. Abruña, E. Maisonhaute, C. Amatore, *Anal. Chem.* **2003**, *75*, 3962–3971.
- [306] A. J. Bard, L. R. Faulkner, *Electrochemical Methods, Fundamentals and Applications*, 2 ed., Wiley, New York, **2001**.
- [307] X. Xiao, A. J. Bard, *J. Am. Chem. Soc.* **2007**, *129*, 9610–9612.
- [308] S. Chen, A. Kucernak, *Electrochem. Commun.* **2002**, *4*, 80–85.
- [309] S. Chen, A. Kucernak, *J. Phys. Chem. B* **2004**, *108*, 3262–3276.
- [310] R. Tel-Vered, A. J. Bard, *J. Phys. Chem. B* **2006**, *110*, 25279–25287.
- [311] J. Lakubub, A. Pouliwe, A. Kamasah, C. Yang, P. Sun, *Electroanalysis* **2011**, *23*, 2270–2274.

- [312] N. Nioradze, R. Chen, J. Kim, M. Shen, P. Santhosh, S. Amemiya, *Anal. Chem.* **2013**, 85, 6198–6202.
- [313] R. A. Lazenby, K. McKelvey, M. Peruffo, M. Baghdadi, P. R. Unwin, *J. Solid State Electrochem.* **2013**, 17, 2979–2987.
- [314] W. Nogala, J. Velmurugan, M. V. Mirkin, *Anal. Chem.* **2012**, 84, 5192–5197.
- [315] K. McKelvey, B. P. Nadappuram, P. Actis, Y. Takahashi, Y. E. Korchev, T. Matsue, C. Robinson, P. R. Unwin, *Anal. Chem.* **2013**, 85, 7519–7526.
- [316] B. Zhang, J. Galusha, P. G. Shiozawa, G. Wang, A. J. Bergren, R. M. Jones, R. J. White, E. N. Ervin, C. C. Cauley, H. S. White, *Anal. Chem.* **2007**, 79, 4778–4787.
- [317] J. Meier, J. Schiøtz, P. Liu, J. K. Nørskov, U. Stimming, *Chem. Phys. Lett.* **2004**, 390, 440–444.
- [318] General Discussion, *Faraday Discuss.* **2002**, 121, 441–462.
- [319] M. Heyrovsky, J. Jirkovsky, *Langmuir* **1995**, 11, 4288–4292.
- [320] M. Heyrovsky, J. Jirkovsky, B. R. Mueller, *Langmuir* **1995**, 11, 4293–4299.
- [321] M. Heyrovsky, J. Jirkovsky, M. Struplova-Bartackova, *Langmuir* **1995**, 11, 4300–4308.
- [322] M. Heyrovsky, J. Jirkovsky, M. Struplova-Bartackova, *Langmuir* **1995**, 11, 4309–4312.
- [323] A. V. Korshunov, M. Heyrovský, *Electroanalysis* **2006**, 18, 423–426.
- [324] B. M. Quinn, P. G. van't Ho, S. G. Lemay, *J. Am. Chem. Soc.* **2004**, 126, 8360–8361.
- [325] S. E. Fosdick, M. J. Anderson, E. G. Nettleton, R. M. Crooks, *J. Am. Chem. Soc.* **2013**, 135, 5994–5997.
- [326] X. Xiao, F.-R. F. Fan, J. Zhou, A. J. Bard, *J. Am. Chem. Soc.* **2008**, 130, 16669–16677.
- [327] X. Xiao, S. Pan, J. S. Jang, F.-R. F. Fan, A. J. Bard, *J. Phys. Chem. C* **2009**, 113, 14978–14982.
- [328] S. E. F. Kleijn, B. Serrano-Bou, A. I. Yanson, M. T. M. Koper, *Langmuir* **2013**, 29, 2054–2064.
- [329] R. Dasari, D. A. Robinson, K. J. Stevenson, *J. Am. Chem. Soc.* **2013**, 135, 570–573.
- [330] P. V. Dudin, P. R. Unwin, J. V. Macpherson, *Phys. Chem. Chem. Phys.* **2011**, 13, 17146–17152.
- [331] L. Aldous, R. G. Compton, *Phys. Chem. Chem. Phys.* **2011**, 13, 5279–5287.
- [332] M. M. Ardakani, M. A. Karimi, M. M. Zare, S. M. Mirdehghan, *Int. J. Electrochem. Sci.* **2008**, 3, 246–258.
- [333] H. R. Zare, N. Nasirizadeh, *Electroanalysis* **2006**, 18, 507–512.
- [334] J. Kunze, I. Burgess, R. Nichols, C. Buess-Herman, J. Lipkowsky, *J. Electroanal. Chem.* **2007**, 599, 147–159.
- [335] G. A. Attard, J.-Y. Ye, P. Jenkins, F. J. Vidal-Iglesias, E. Herrero, S.-G. Sun, *J. Electroanal. Chem.* **2013**, 688, 249–256.
- [336] H. Zhou, F.-R. F. Fan, A. J. Bard, *J. Phys. Chem. Lett.* **2010**, 1, 2671–2674.
- [337] S. J. Kwon, F.-R. F. Fan, A. J. Bard, *J. Am. Chem. Soc.* **2010**, 132, 13165–13167.
- [338] S. J. Kwon, A. J. Bard, *J. Am. Chem. Soc.* **2012**, 134, 7102–7108.
- [339] Y.-G. Zhou, N. V. Rees, R. G. Compton, *Angew. Chem.* **2011**, 123, 4305–4307; *Angew. Chem. Int. Ed.* **2011**, 50, 4219–4221.
- [340] N. V. Rees, Y.-G. Zhou, R. G. Compton, *ChemPhysChem* **2011**, 12, 1645–1647.
- [341] Y.-G. Zhou, N. V. Rees, R. G. Compton, *ChemPhysChem* **2011**, 12, 2085–2087.
- [342] Y.-G. Zhou, N. V. Rees, R. G. Compton, *Chem. Phys. Lett.* **2011**, 511, 183–186.
- [343] Y.-G. Zhou, N. V. Rees, R. G. Compton, *Chem. Phys. Lett.* **2011**, 514, 291–293.
- [344] E. J. E. Stuart, N. V. Rees, R. G. Compton, *Chem. Phys. Lett.* **2012**, 531, 94–97.
- [345] Y.-G. Zhou, N. V. Rees, R. G. Compton, *Chem. Commun.* **2012**, 48, 2510–2512.
- [346] H. Zhou, J. H. Park, F.-R. F. Fan, A. J. Bard, *J. Am. Chem. Soc.* **2012**, 134, 13212–13215.
- [347] N. V. Rees, Y.-G. Zhou, R. G. Compton, *Chem. Phys. Lett.* **2012**, 525–26, 69–71.
- [348] S. J. Kwon, H. Zhou, F.-R. F. Fan, V. Vorobyev, B. Zhang, A. J. Bard, *Phys. Chem. Chem. Phys.* **2011**, 13, 5394–5402.
- [349] E. O. Barnes, R. G. Compton, *J. Electroanal. Chem.* **2013**, 693, 73–78.
- [350] E. J. F. Dickinson, N. V. Rees, R. G. Compton, *Chem. Phys. Lett.* **2012**, 528, 44–48.
- [351] E. J. E. Stuart, Y.-G. Zhou, N. V. Rees, R. G. Compton, *RSC Adv.* **2012**, 2, 12702–12705.
- [352] J. V. Macpherson, D. Wakerley, A. Güell, L. Hutton, T. Miller, A. Bard, *Chem. Commun.* **2013**, 49, 5657–5659.
- [353] K. Huang, A. Anne, M. A. Bahri, C. Demaille, *ACS Nano* **2013**, 7, 4151–4163.
- [354] X. Shan, I. Diez-Perez, L. Wang, P. Wiktor, Y. Gu, L. Zhang, W. Wang, J. Lu, S. Wang, Q. Gong, J. Li, N. Tao, *Nat. Nanotechnol.* **2012**, 7, 668–672.
- [355] X. Shan, X. Huang, K. J. Foley, P. Zhang, K. Chen, S. Wang, N. Tao, *Anal. Chem.* **2010**, 82, 234–240.
- [356] X. Shan, U. Patel, S. Wang, R. Iglesias, N. Tao, *Science* **2010**, 327, 1363–1366.
- [357] A. Kumar, F. Ciucci, A. N. Morozovska, S. V. Kalinin, S. Jesse, *Nat. Chem.* **2011**, 3, 707–713.